

# In-flight experience of the Mars Science Laboratory Guidance, Navigation, and Control system for Entry, Descent, and Landing

Miguel San Martin<sup>1</sup>  · Gavin F. Mendeck<sup>2</sup> · Paul B. Brugarolas<sup>1</sup> · Gurkirpal Singh<sup>1</sup> ·  
Frederick Serricchio<sup>1</sup> · Steven W. Lee<sup>1</sup> · Edward C. Wong<sup>1</sup> · John C. Essmiller<sup>1</sup>

Received: 15 January 2015 / Revised: 3 April 2015 / Accepted: 14 April 2015 / Published online: 30 May 2015  
© CEAS 2015

**Abstract** The Mars Science Laboratory (MSL) project successfully landed the rover Curiosity in Gale crater in August 5, 2012, thus demonstrating and validating a series of technical innovations and advances which resulted in a quantum leap in Entry, Descent, and Landing (EDL) performance relative to previous missions. These included the first use at Mars of Entry Guidance to reduce the size of the landing ellipse and the first use of the SkyCrane landing architecture to enable the placement of a 1 ton class rover on the surface of the red planet. Both of these advances required innovations in the design, analysis and testing of the Guidance, Navigation, and Control system. This paper will start with a high-level description of the MSL EDL/GN&C system design and performance requirements, followed by a brief discussion of the risks and uncertainties as they were understood prior to landing, and the actual in-flight GN&C performance as reconstructed from telemetry. Finally, this paper will address areas of improvements for future Mars EDL missions.

**Keywords** EDL · GN&C · Mars · NASA · MSL · Curiosity

## 1 Introduction

Two main challenges drove the design and implementation of the Mars Science Laboratory (MSL) Entry, Descent, and

This paper is based on a presentation at the 9th International ESA Conference on Guidance, Navigation & Control Systems, June 2–6, 2014, Porto, Portugal.

✉ Miguel San Martin  
alejandro.m.sanmartin@jpl.nasa.gov

<sup>1</sup> Jet Propulsion Laboratory, California Institute of Technology, Pasadena, CA 91109, USA

<sup>2</sup> NASA Johnson Space Center, Houston, TX 77058, USA

Landing (EDL) system: the large reduction in the size of the Landing Ellipse and the large increase in the Landed Mass as compared to previous missions [1, 2].

The reduction in the size of the Landing Ellipse was dictated by the desire to give scientists more choices when selecting sites of great scientific value and still safe for landing the Curiosity rover. Scientists made maximum use of this new capability when they selected Gale Crater as the landing site, boldly placing the ellipse at the crater's floor between the dangers of its rim at one side and Mt Sharp (a 5.5 km high mountain in its center) at the other (Fig. 1). Figure 2 illustrates the reduction of the landing ellipses since Viking against a picture of Gale Crater. Only MSL landing ellipse can fit in the tight space within the crater.

The increase in the landed mass capability of MSL EDL was dictated by the mass of the Curiosity rover, which itself was driven by the size and complexity of its scientific instruments and the need for improved mobility. Figure 3 compares the size of Curiosity against the previous Mars rovers.

To meet the first challenge, Landing Ellipse reduction, MSL employed the first use at Mars of Entry Guidance. This technique, which was used successfully by Gemini and Apollo to guide the capsules precisely and safely through the Earth's atmosphere to land closely to recovery assets, requires a lifting capsule (Fig. 4), on-board guidance, navigation and control software, and an RCS propulsion system to stabilize and control the roll of the capsule to point its Lift vector as commanded by the on-board guidance function.

To meet the challenge of placing, a 1 ton class rover with the size of a small car on the surface of Mars, MSL had to invent a totally new landing architecture: the SkyCrane (Fig. 5). This architecture solved the rover-egress problem (i.e., how to lower the rover from the top deck of a Viking style legged lander) by placing the rover on the surface of

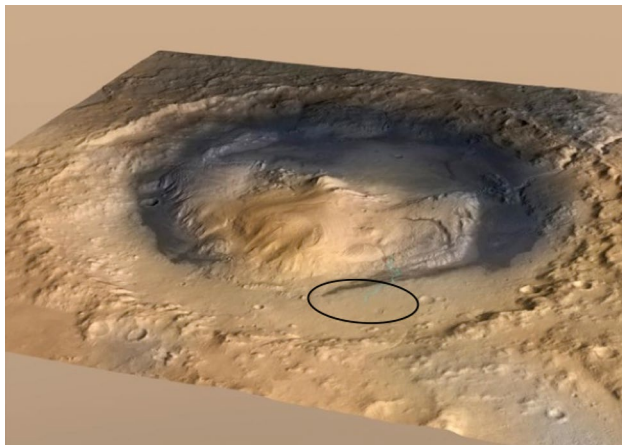


**Fig. 1** Gale crater and Curiosity's Landing Ellipse

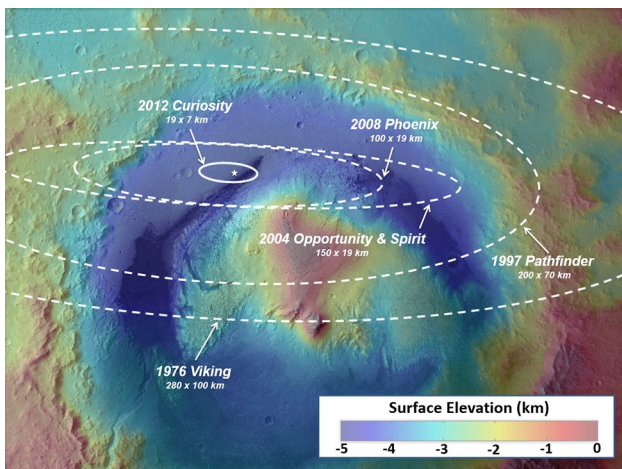


**Fig. 2** Gale crater and Landing Ellipses for several missions (NASA/JPL-Caltech)

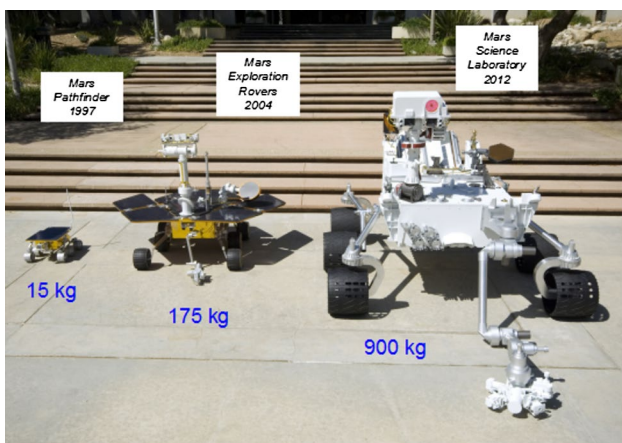


**Fig. 3** Comparison of MSL/Curiosity Rover with previous ones

the Red Planet directly on its wheels while suspended by bristles from a propulsive Descent Stage. The SkyCrane, however, solved this mechanical rover-egress problem at the cost of requiring GN&C to control and stabilize the two-body pendulous system, plus levying on it the softest touchdown velocity requirements ever attempted on Mars (Fig. 6).

This paper will first give a high level description of the design of MSL EDL, emphasizing the GN&C aspects, followed by a description of the salient aspects of EDL GN&C in-flight performance as reconstructed from the detailed telemetry gathered during landing and down-linked to Earth in the days that followed, and ending with a section on future updates and improvements to the MSL GN&C architecture that are currently being investigated.

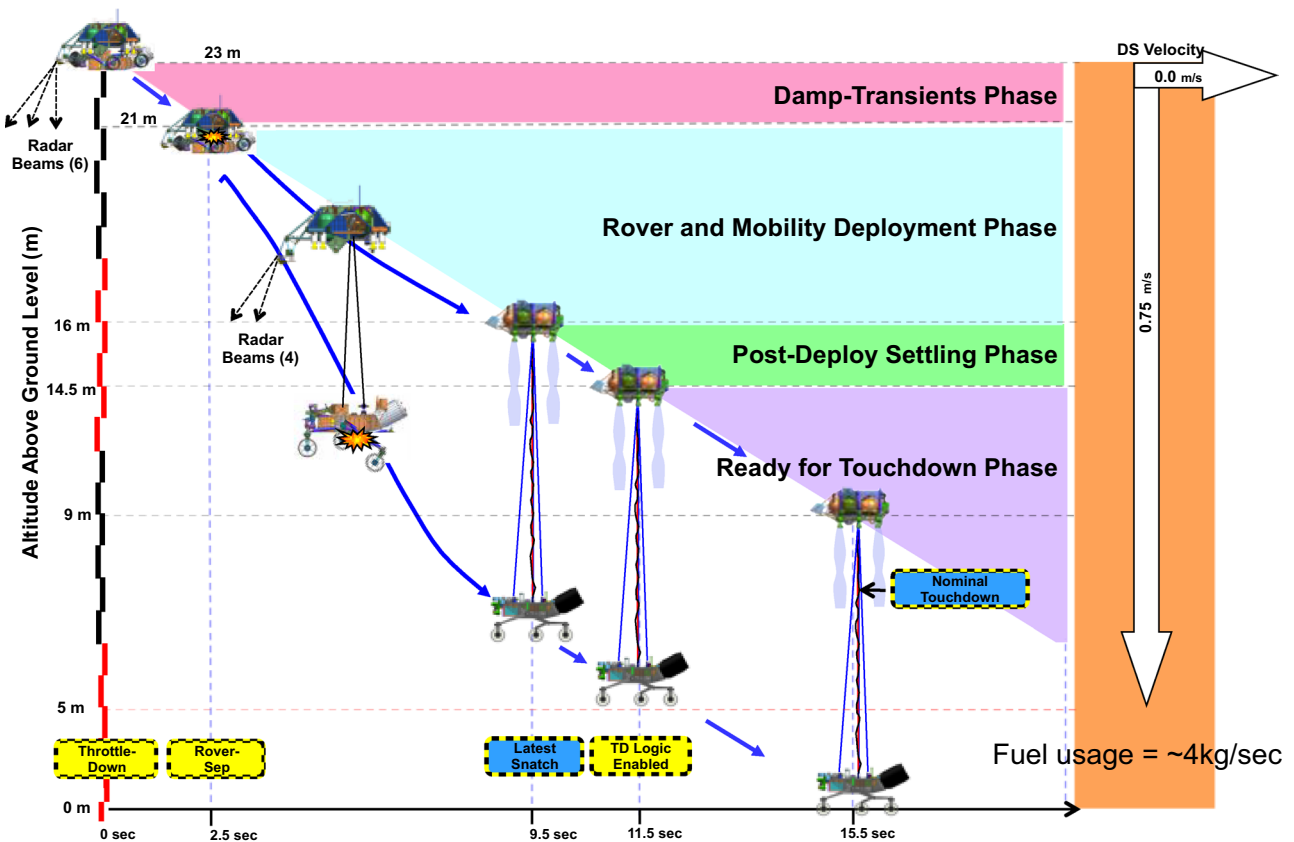
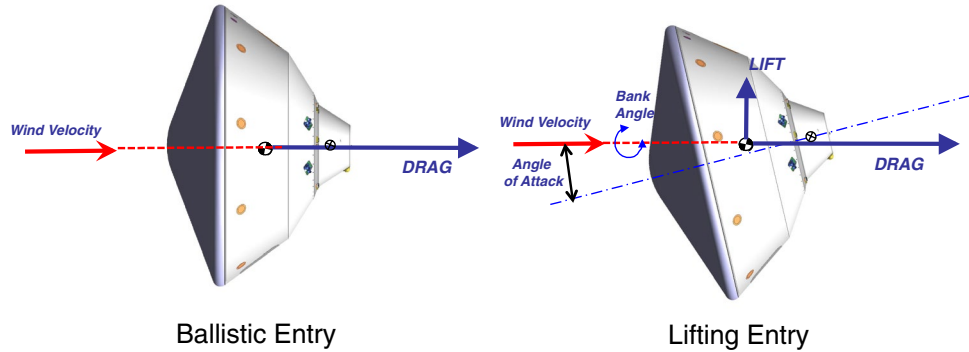
## 2 Entry, Descent, and Landing system design

Figure 7 illustrates the three phases of EDL. The Entry phase starts with the spacecraft arriving with a velocity of 6.1 km/s at Entry Interface, a point semi-arbitrarily chosen to be at 125 km altitude, the very upper layers of the atmosphere, and ending as soon as the conditions to safely open the parachute are achieved, which for Curiosity occurs at Mach 1.7. During this phase, 99 % of the starting kinetic energy is dissipated through aerodynamic braking, which subjects the entry capsule to the largest decelerations and heating environments, the second handled by the Thermal Protection System (TPS). This phase is also the most important in determining the size of the Landing Ellipse. The Entry phase is followed by the Parachute Descent phase, which starts with the opening of the parachute, during which about 1 % of the initial kinetic energy is dissipated. Given that the Martian atmospheric density is only 1 % that of Earth, the terminal descent velocity during this phase, between 60 and 100 m/s, is still too high for a landing, necessitating a third braking phase, the Landing Phase, in which the propulsion system takes the vehicle all the way until it is safely on the ground with zero ground speed and altitude.

### 2.1 Entry phase

The MSL Entry Guidance algorithm was based on the one used by Apollo in the 1960s and is described in detail in reference [3]. To achieve a smaller landing ellipse, the guidance algorithm adjusts the trajectory of the vehicle by commanding the direction of the capsule's lift vector, an aerodynamic force perpendicular to the atmosphere relative velocity vector (Fig. 4), through bank maneuvers implemented by the Entry Controller using the Reaction Control System. It has two phases: Range Control and Heading Alignment.

**Fig. 4** Ballistic versus Lifting Entry



**Fig. 5** SkyCrane phase

During Range Control, which starts when the accelerometers sense 0.2 g and ends when the navigated velocity is <1100 m/s, a predictor–corrector algorithm commands bank angles to change the Lift force direction to control range while keeping cross-range errors within a given corridor by performing, nominally three, bank-reversals (Fig. 8). If the algorithm predicts that the spacecraft is going to be short of the target, then it commands more lift-up to reduce drag (by going to the higher altitudes with lower atmospheric density) and fly longer. If the algorithm predicts that the spacecraft is going to overshoot the target, it then commands

lower lift-up to increase drag (by going to the lower altitudes with higher atmospheric density) and fly shorter.

To achieve this, guidance first computes the predicted range-to-go ( $R_p$ ), calculated as the sum of the filtered drag and altitude rate errors with respect to the nominal reference trajectory profile values, weighted by the corresponding partial derivative gains, plus the reference range-to-go at this velocity (1), Fig. 9.

$$R_p = R_{\text{ref}} + \frac{\partial R}{\partial D}(D - D_{\text{ref}}) + \frac{\partial R}{\partial \dot{r}}(\dot{r} - \dot{r}_{\text{ref}}) \quad (1)$$

**Fig. 6** Comparison of MSL/Curiosity touchdown speed requirements with previous missions

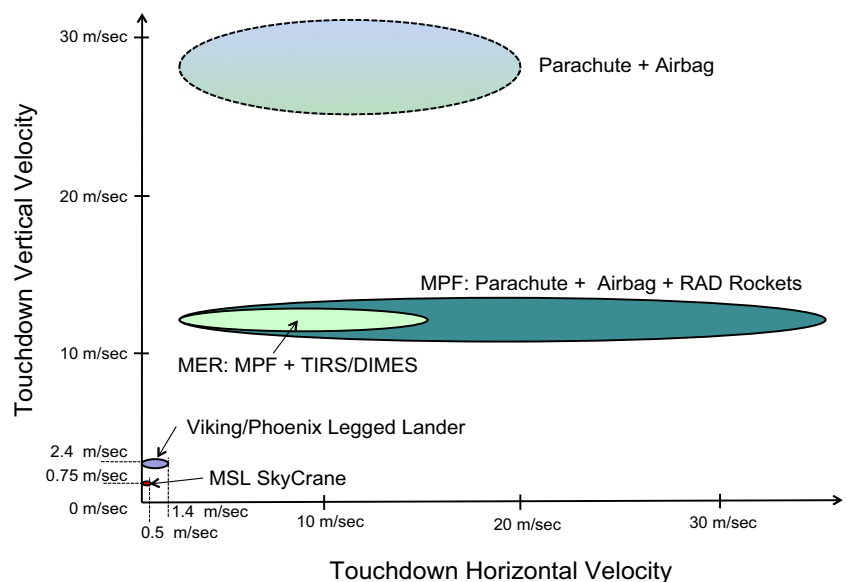


**Fig. 7** MSL/Curiosity Entry Descent and Landing phases

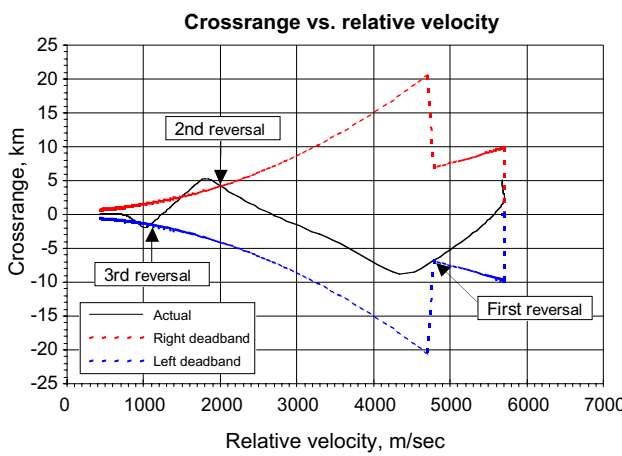
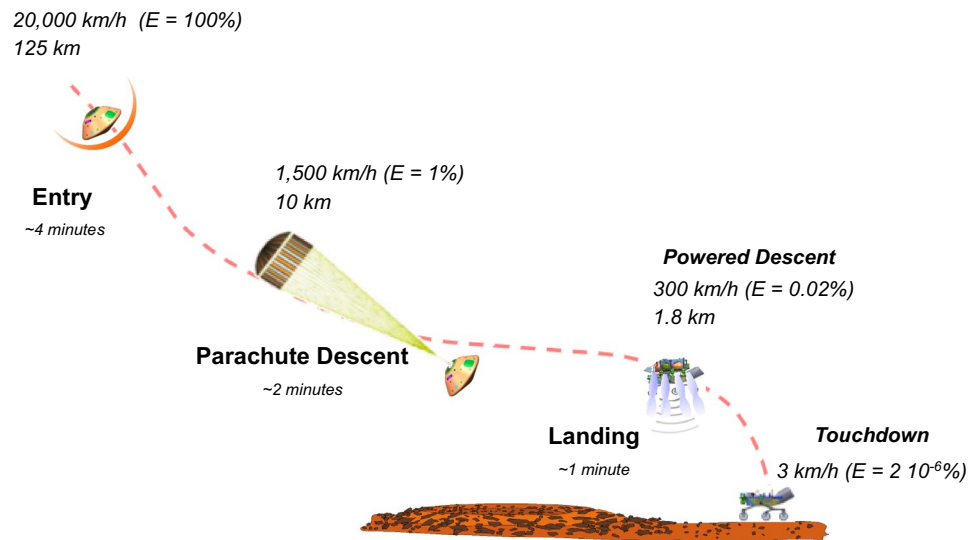


**Fig. 8** Crossrange management during the Guidance Range Control phase

The commanded vertical component of the lift-to-drag ( $L/D$ ) ratio is then calculated as a function of the difference between the actual ( $R$ ) and predicted range-to-go ( $R_p$ ), i.e., the downrange error. The difference is then converted to a change in vertical  $L/D$  commanded that is then applied to the reference vertical  $L/D$  at this velocity in (2).

$$\left(\frac{L}{D}\right)_C = \left(\frac{L}{D}\right)_{\text{ref}} + \frac{K_3(R - R_p)}{\partial R / \partial (L/D)} \quad (2)$$

Finally, the commanded bank angle ( $\Phi_C$ ) is then calculated using the commanded vertical- $L/D$  and the estimated  $L/D$  as in (3).

$$\Phi_C = \cos^{-1} \left( \frac{(L/D)_C}{(L/D)_{\text{est}}} \right) \times K_2 \quad (3)$$

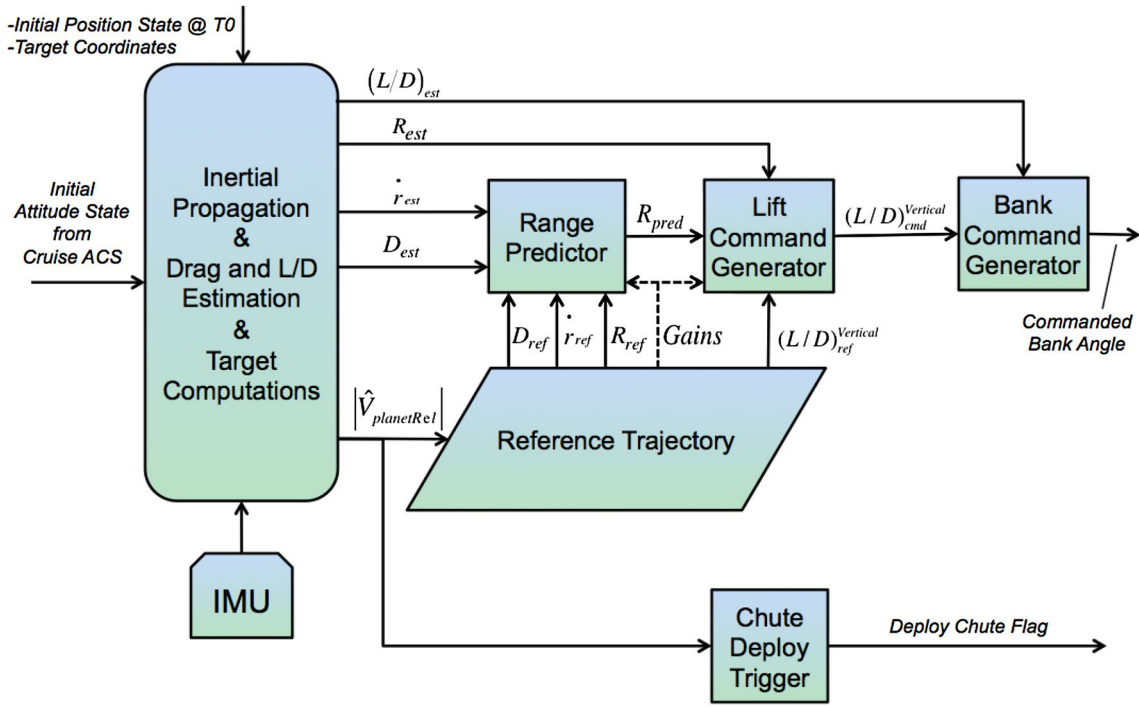


**Fig. 9** Entry Guidance Algorithm: Range Control

The sensed drag acceleration in (1) and estimated lift-to-drag ratio in (3) are derived from accelerometer measurements and smoothed by first order filters. The  $K_2$  term in Eq. 3 is the bank directional control ( $\pm 1$ ), which is reversed each time the crossrange error exceeds the bank-reversal deadbands that are a function of velocity (Fig. 8).

During Heading Alignment, which starts after Range Control and ends with the start of the events leading to parachute deploy, Entry Guidance commands bank angle only to reduce the cross-track position errors that were left from the Range Control phase, and those that are currently being introduced. Range error is left uncontrolled during this phase because Range Control efficacy is diminished at velocities lower than 1100 m/s. The commanded bank angle is proportional to the current azimuth error to the target, defined by the crossrange,  $R_c$ , and downrange,  $R$ , to the target as shown in (4).

$$\Phi_C = \tan^{-1} \left( \frac{R_c}{R} \right) K_4 \quad (4)$$

As mentioned, the commanded bank angle is not allowed to output a value greater than  $30^\circ$  magnitude in this phase to prevent substantial loss of the deploy altitude while still allowing some reduction of crossrange error.  $K_4$  is the proportional controller to the azimuth error.

During this phase, GN&C provides RCS based 3-axis Attitude Control functionality to stabilize the plant and control the direction of the Lift vector during atmospheric

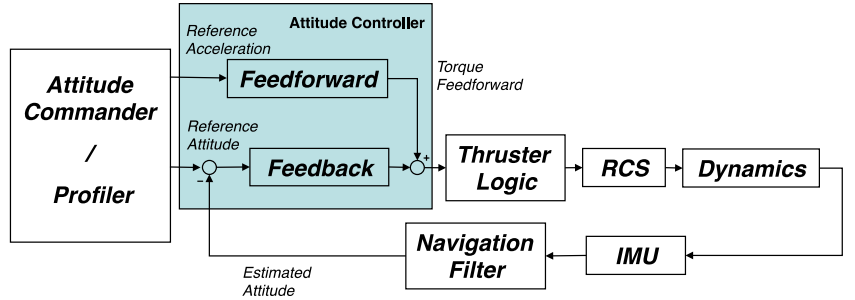
flight. The same controller is used during exo-atmospheric flight, prior to Entry Interface, to spin-down the capsule from its cruise 2 RPM rate, and to turn it to the correct attitude for entry (i.e., angle-of-attack consistent with the atmosphere relative velocity).

The plant stabilization mentioned above is required because the capsule aerodynamics experiences a dynamic instability (unstable  $C_{mq}$ ) at supersonic speeds. This can be problematic because it can result in growing capsule oscillations starting just before parachute deployment, which can exceed the maximum capsule angle-of-attack limit required for successful deployment and inflation of the chute.

The Entry Controller was implemented as a hybrid PD/dead-bands controller with feed-forward and RCS pulse-width modulation (Fig. 10) [4, 8]. All commanded turns (i.e., turn-to-entry, bank-reversals, turn-to-heading-alignment) were profiled and fed-forward, and they were implemented as coordinated turns (i.e., about the capsule trim axis).

During the Entry Phase, GN&C provides triggers to signal the start of the Range Control Phase, the start of the Heading Alignment phase, the start of the activities leading to Parachute Deployment, and the time of proper Parachute Deploy which was targeted to occur at 1.7 Mach. The start of the Range Control phase trigger is an acceleration trigger that activates when the drag acceleration is larger than 0.2 g. The three triggers that follow are planet-relative velocity magnitude triggers that use inertially propagated

**Fig. 10** Entry Attitude Controller



velocity generated by the Navigation Filter initialized with a ground-computed 6-axis navigation state (position and velocity) at a given epoch (9 min prior to Entry Interface).

## 2.2 Parachute Descent phase

During this phase, GN&C's main role is to determine the time to separate the heatshield (Heatshield Separation Trigger), the time to prime the Mars Landing Engines (MLE), and the time to separate from the backshell (Powered Descent Start Trigger), all based on Vehicle state estimates generated by the Navigation Filter.

The Heatshield separation Trigger is a planet-relative velocity magnitude trigger like the ones used during the Entry Phase, but with a small twist to make it less sensitive to cruise attitude initialization errors. Basically, to maximize timeline margin, the goal is to separate the heatshield as soon as the aerodynamic conditions guarantees that a safe no re-contacting heatshield separation will take place. Just as it is the case for the parachute deployment, the appropriate aerodynamic conditions are a function of Mach number, which for MSL's safe heatshield deployment is a velocity of <0.65 Mach. However, since there is no Mach airspeed sensor in the spacecraft, the trigger must fire on the equivalent inertially propagated planet-relative velocity magnitude.

However, early in the development of MSL, an unacceptably large number of Monte Carlo simulation failures were encountered and attributed to large errors in the inertially propagated velocity estimate which were causing large delays in the heatshield separation trigger activation, thus resulting in insufficient time to complete all the EDL activities before touchdown (i.e., timeline failure). Further analysis indicated that these velocity estimation errors were due to errors in the attitude knowledge initialization that took place at the start of EDL (attitude knowledge is transferred from the Attitude Estimator in the Cruise Attitude Control System to the EDL inertial propagator just before Cruise Stage separation, 10 min before Entry Interface).

The solution to this problem became obvious when further analysis of the Monte Carlo simulation results found that the velocity estimation error vectors, caused by attitude

initialization errors, formed a plane in space closely perpendicular to the spacecraft's planet-relative velocity at Entry Interface (this is not surprising given that this type of velocity estimation error can be approximated by the cross product of the attitude initialization error and the spacecraft planet-relative velocity at Entry Interface, the last with a practically constant fixed direction even with navigation delivery errors included). This observation led to the development of the Dot Product Heatshield Separation Trigger. Basically, instead of taking the magnitude of the 3-axis estimated spacecraft velocity vector before comparing it to the trigger scalar threshold, the new trigger takes the dot product of the estimated velocity vector with a unit-vector perpendicular to the velocity estimation error plane described above, thus making this trigger virtually insensitive to the estimated velocity errors due to attitude initialization errors (while there are analytical expressions to compute the perpendicular to this error plane, we chose to determine it from estimated velocity error plane fits of Monte Carlo simulation results).

The MLE Priming Trigger is an altitude trigger that is activated when the estimated altitude falls below 3 km, which gives ample time to prime the propulsion feed system before Powered Descent start, thus avoiding damaging water-hammer effects.

The Powered Descent Start Trigger computes the appropriate altitude to separate from the Backshell and start Powered Descent, based on the estimated vertical velocity. At a higher vertical velocity, the trigger activates at a higher altitude to avoid exceeding the control authority of the MLE's. At a lower vertical velocity, this trigger activates at a lower altitude to avoid excessive fuel consumption. The nominal velocity and altitude values for this trigger are 80 m/s and 1.6 km.

Both altitude and ground relative velocity are provided by the Navigation Filter by fusing measurements from the landing radar (or TDS, Terminal Descent sensor) and the Inertial Measurement Unit (IMU). The Navigation Filter first has to converge and produce the first Altitude and 3-axis Ground-Relative Velocity Solution before the GN&C executive starts calling the MLE Priming Trigger. The Navigation Filter requires a minimum of 5 s of valid radar data to converge. The time between when the Nav

Filter converges and when the solution is first needed (i.e., MLE priming) varies substantially with the altitude of the landing site; for Gale Crater the mean time between Nav Filter convergence and first use was 45 s.

### 2.3 Landing phase

The first part of this phase, from backshell separation at 1.6 km up to 23 m altitude, is basically very similar to previous soft-landers such as Viking. It is a single body controlled in six degrees-of-freedom by 8 throttleable engines, and with altitude and 3-axis ground relative velocity provided by a Navigation Filter using measurements from landing radar and the IMU.

Backshell separation is followed by a one second of free fall to avoid short term re-contact with the backshell, a 0.2 s of open-loop MLE warm up at 20 % throttle, a profiled

de-tumble maneuver to null the attitude-rates present at backshell separation, and a profiled turn to the desired attitude at the start of the translational guidance [5, 6]. These two close-loop attitude maneuvers are allocated 2.5 s for their completion.

Translational guidance is made up of four phases (Fig. 11), each one with a different guidance objective to be achieved at the end of the given phase. For each phase, a polynomial function provides a reference trajectory (position, attitude, acceleration magnitude) to be followed closed loop by the Power Descent translational controllers (Fig. 12); the polynomial coefficients are computed at the beginning of each phase by solving a two-point boundary-value problem [5].

The powered approach guidance phase objective is to zero the horizontal velocity, reduce the descent velocity to 32 m/s, align the lander attitude with the vertical, and perform a 300 m divert maneuver to avoid the parachute/

**Fig. 11** Powered Descent phases

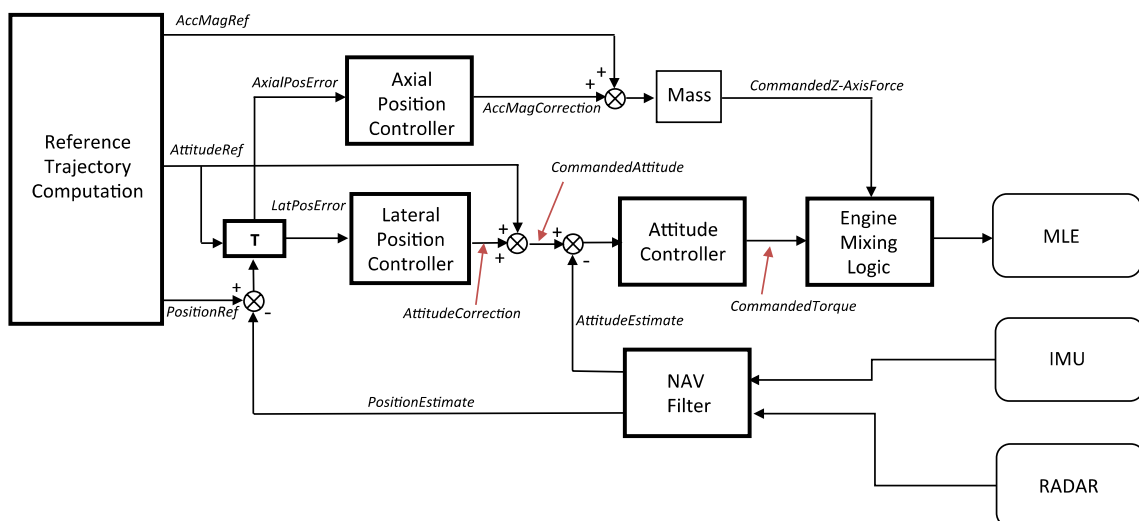
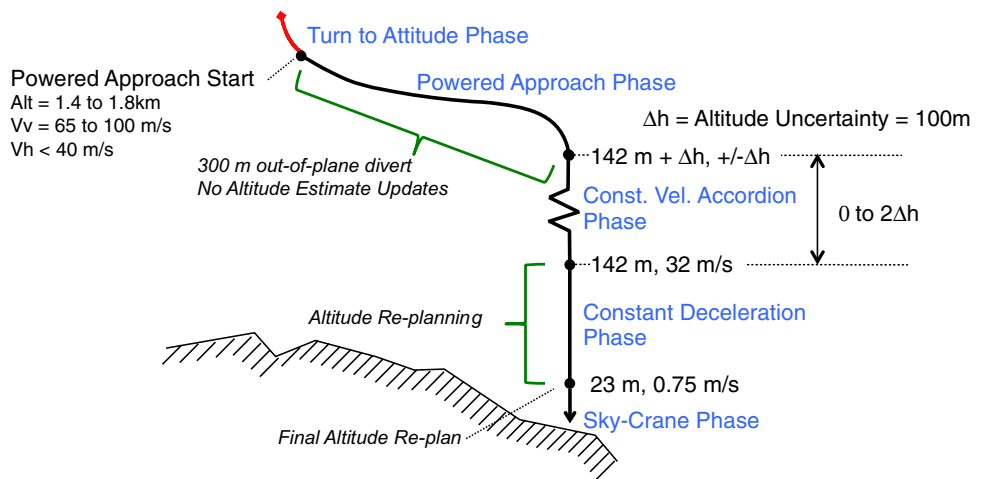


**Fig. 12** Powered Descent guidance and controllers

backshell from re-contacting with the lander. As far as altitude is concerned, the Power Approach phase aims at a point over the ground that is the desired altitude at the beginning of the Constant Deceleration phase, 142 m, plus a  $\Delta h$  that corresponds to the altitude uncertainty (due to radar error and terrain relief features) at the beginning of the phase when the reference trajectory polynomial was computed. During Powered Approach, the guidance law flies to the “inertial” point described above without introducing changes due to improvements in the altitude estimate knowledge, as the spacecraft gets closer to the terrain in which it is going to land.

The Constant Velocity Accordion phase allocates altitude margin as an “accordion” to compensate for the altitude measurement error introduced at the beginning of Powered Approach. MSL flew with  $\Delta h = 100$  m to accommodate approximately  $\pm 40$  m (3-sigma) of altitude error as determined by a Gale Crater EDL Monte Carlo simulation which included a high fidelity terrain model derived from Mars Reconnaissance Orbiter High Resolution Imaging Science Experiment (HiRISE) imagery.

During the Constant Deceleration phase, the vertical velocity of the lander is brought down to the 0.75 m/s touchdown velocity, while continuing to follow a vertical profile (i.e., zero horizontal velocity). During this phase, there is also a reference trajectory re-planning capability used to adjust for minor changes in the altitude knowledge.

The SkyCrane phase starts at an altitude of 23 m, with the lander already at the right ground relative velocity required for touchdown: 0.75 m/s vertical velocity and 0 m/s horizontal velocity. Since there is no need for large decelerations during and after this phase, four engines are throttled down to keep the remaining ones at a throttle level comfortably higher than the minimum allowed. The throttle-down to four engines occurs at the start of the SkyCrane phase and 2.5 s are allocated for the transients to subside before proceeding with Rover Separation (Fig. 5).

The final guidance trajectory planning also occurs at the beginning of the SkyCrane phase using the latest knowledge of altitude at that point. This planned trajectory allocates a 5 m touchdown accordion to compensate for errors in the altitude knowledge at the start of this phase and the propagation errors incurred after that.

During this phase, GN&C keeps the vehicle controlled and descending with the same constant velocity profile, even in the presence of the large transients caused by the Rover separation, Mobility deployments, and the touchdown event itself. All of these transients are handled by the GN&C feedback loops.

During the touchdown event, the constant velocity GN&C close-loop function continues until the full weight of the rover is supported by the ground, at which point the Touchdown Detection Trigger is activated. The Touchdown Detection

Trigger works essentially by monitoring the commanded engine throttle required to support the system against gravity as it descends at constant velocity. When the engine throttle command is reduced to a value consistent with the weight of the Descent Stage only, then touchdown is declared. Because the weight of the Rover is roughly the same as the weight of the Descent Stage, the throttle command value is reduced by 50 % through the touchdown event, thus providing a very strong, unambiguous, and persistent signal.

The touchdown trigger starts the Fly-Away sequence in which GN&C first brings the vehicle to a stop with a constant vertical deceleration profile and then enters a zero velocity hold mode until Descent Stage control is transferred to the Fly-Away controller.

The Fly-Away controller is a simple GN&C algorithm designed to fly the Descent Stage to impact at a safe distance ( $\sim 600$  m) from the Rover. This algorithm is hosted in the MLE Motor Controller computer (which also provides servo control for the MLE throttle valves) in the Descent Stage (the rest of EDL/GN&C flight software was executed in the Rover computer) and uses IMU attitude-rate measurements to close the loop on an attitude profile that first turns the Descent Stage  $\sim 45^\circ$  from the vertical and then maintains that attitude while the engines are commanded to throttled up for a fixed duration of time in order to impart the desired delta-velocity that takes the Descent stage far from the rover. At the end of that period the MLE’s are commanded to shut down and the Descent Stage follows a ballistic trajectory until impact.

Throughout all Powered Descent, six feedback control loops act together to follow the reference trajectory dictated by the guidance law, using position and attitude estimates from the Navigation Filter (Fig. 12).

The position error is computed from the Navigation Filter estimated position and the Reference Trajectory desired position, and converted into the Reference Trajectory Descent Stage frame. In this frame, the z-axis of the position error is along the Descent Stage thrust direction (i.e., the vertical axis in its landing orientation) and is used by the Axial Controller to command the translational acceleration along that axis, which is directly controlled by the MLE throttle valves. The x and y position errors go to the lateral controller that commands lateral acceleration changes by commanding pitch and yaw attitude deltas from the reference attitude. The resulting Descent Stage attitude is then commanded to the Attitude Controller, which request torques to the Engine Mixing logic, which are ultimately achieved by differential MLE throttle commands.

The axial position loop and the three Attitude control loops have bandwidths in the 1 Hz range for good transient response and disturbance rejection. The two Lateral control loops have bandwidths in the 0.2 Hz range, low enough to maintain frequency separation with the inner 1 Hz attitude loops. All loops run at a 64 Hz sample rate to preserve

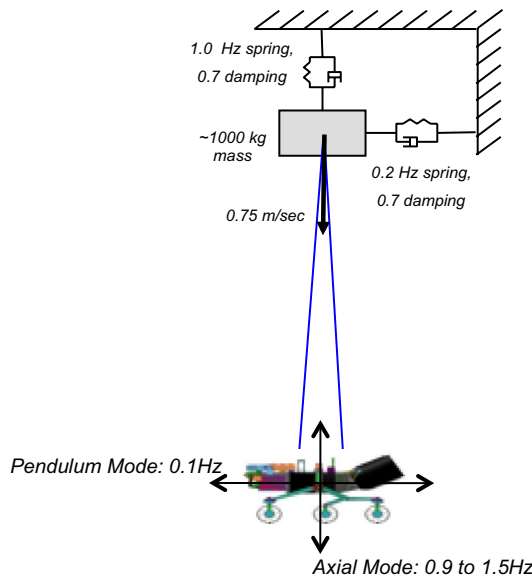


**Fig. 13** SkyCrane modes and translational control bandwidths

phase margins for phase stabilization of the SkyCrane pendulum and axial modes (see below).

The structural modes during the single-body and the two-body SkyCrane phases were above 16 Hz and gain stabilized. Slosh modes, at above 2 Hz and heavily damped thanks to the use of diaphragms in the fuel tanks, were also

gain stabilized. The bridle axial mode at ~0.9–1.5 Hz and pendulum modes at ~0.1 Hz were both phase stabilized (Fig. 13). No special control features were required during the two-body SkyCrane phase, beyond the capability to reschedule different controller gains.

#### 2.4 GN&C relevant hardware

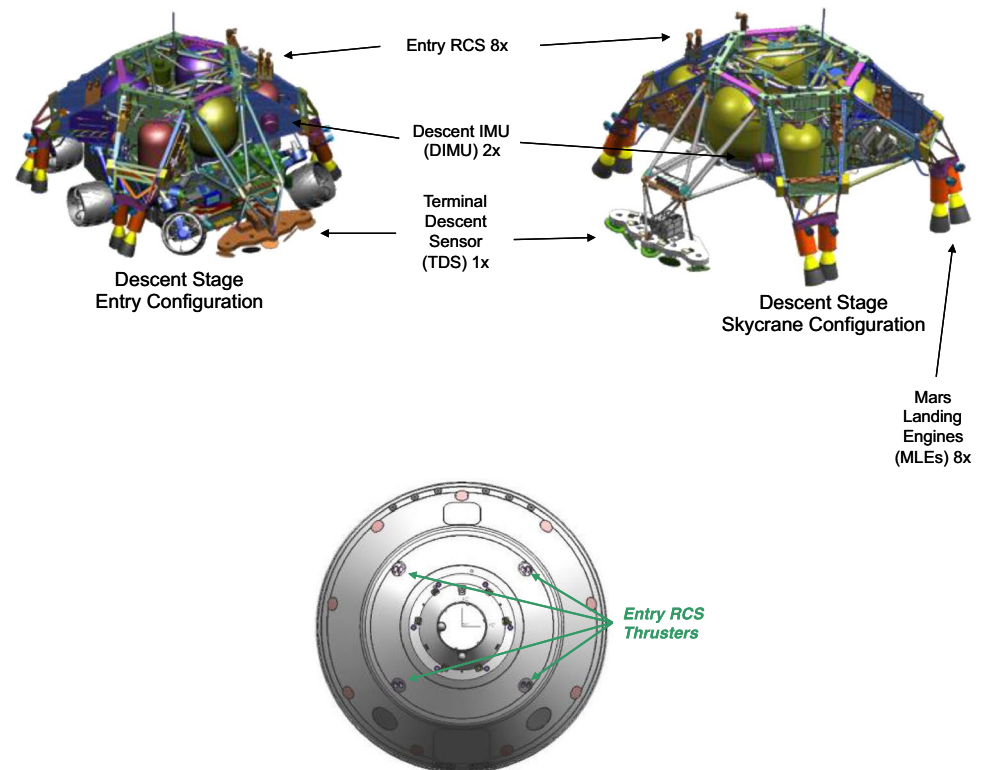
To perform the functions described in the previous section, GN&C required a set of state-of-the-art sensors and actuators, all mounted on the Descent Stage or DS (Fig. 14).

As is typical in previous Mars soft-landers like Viking and Phoenix, MSL GN&C requires an IMU to measure attitude rate and translational acceleration, and a landing radar, to measure 3-axis ground-relative velocity and altitude.

The IMU is the Honeywell MIMU and there are two located on the Descent Stage for redundancy, as can be seen in Fig. 14 (DIMU for Descent Stage IMU). The MIMU is a space-qualified unit that has flown successfully in space numerous times, including in the Phoenix mission that landed successfully on Mars in 2008 performing a similar function as with MSL.

MSL developed a new landing radar, the (TDS), implementing a space-qualified design which employed the latest technology to achieve the accuracy and robustness required by the SkyCrane architecture and the reliability dictated

**Fig. 14** GN&C relevant hardware



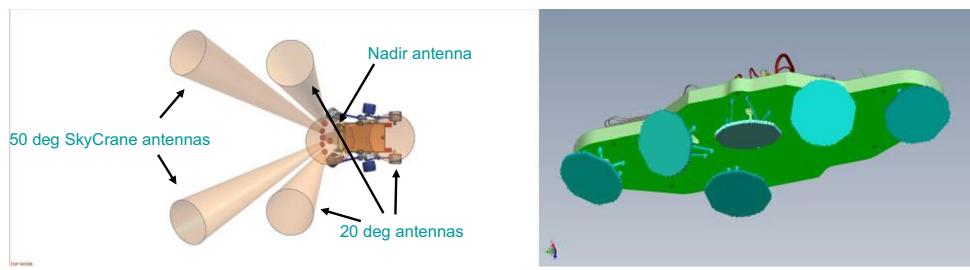


**Fig. 15** TDS antenna configuration

by a flagship mission. The TDS is a Ka-band (35.75 GHz) pulse-pair Doppler radar design. It measures ground-relative velocity and slant-range along the boresight of each of its six narrow beam ( $\sim 3.5^\circ$  width) antennas, at a rate of 20 measurements per second (where each measurement is a velocity/slant-range pair for a single antenna beam).

The antenna configuration consists of a nadir beam, for maximum altitude measurement accuracy during vertical flight prior to touchdown, three  $20^\circ$  beams, and two  $50^\circ$  beams which were added to guarantee that at least those two beams would not experience multipath interference from the rover during the SkyCrane phase (Figs. 14, 15). The beam sequence is programmable and is changed by commands from the EDL Executive, which selects the optimal beam sequence for the current phase of flight. For example, during the SkyCrane, the beam sequence consists of only the two  $50^\circ$  beams since the other beams were at risk of multipath interference with the rover. We call these the SkyCrane beams or antennas.

During exo-atmospheric flight and entry, eight RCS thrusters mounted on the Descent Stage and protruding through the backshell, were used for attitude control (Fig. 14) [7, 8]. Each provided 150 N of force during exo-atmospheric flight, and 250 N when the propulsion system was pressurized at Entry Interface.

During Powered Descent, eight throttleable Mars Landing Engines (MLE) were used for attitude and translation control (Figs. 14, 16). The MLE's are based on the Viking throttleable-landing-engines which, through a focused technology development program, were successfully revived with some important modifications [7]. The MSL version does not have the 18 small nozzles used in Viking to minimize plume ground pressure since the SkyCrane architecture does not require it. It also has a new cavitating throttle valve that reduces the dependence of the flow rate (i.e., thrust) on downstream pressure drop. The engine can be throttled from a minimum thrust of 400 N to a maximum 3060 N.

The propulsion system is pressurized at Entry Interface thus maintaining a constant thrust level, in both the RCS thrusters and MLE's, despite fuel depletion.



**Fig. 16** MSL Mars Landing Engine (MLE)

### 3 Reconstructed EDL performance

After the successful landing of Curiosity, the EDL team spent several months analyzing in detail the high fidelity telemetry gathered during landing. In this section, we are going to present the most important aspects of what was learnt regarding mainly the GN&C part of EDL.

We start by showing in Fig. 17, a summary of EDL performance by displaying the values of the most important EDL metrics. The metrics with flight values less than 1-sigma of the expectation are shown in green, the ones between 2- and 3-sigma in yellow and, finally the ones above 3-sigma in red. Red in itself does not mean closeness to mission failure but simply that the flight value was larger or smaller than expected in the 99 % (or 1 %) sense. Actually, as it will be explained later, all the red quantities: Nav Filter convergence altitude, vertical touchdown velocity, and fuel usage, ended being “wrong” in the “right” direction.

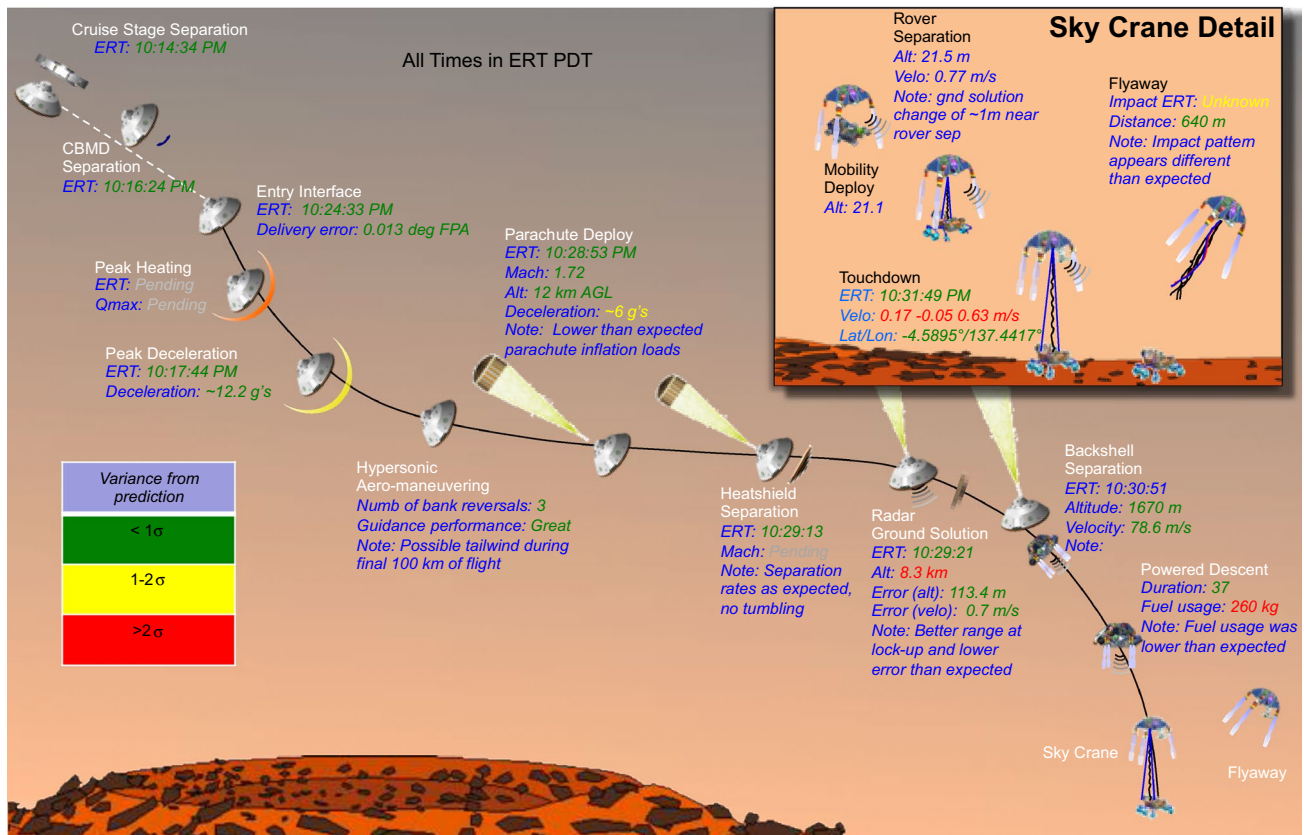


**Fig. 17** As flown EDL metrics (Courtesy of Steve Sell, Jet Propulsion Laboratory)

### 3.1 Navigation state initialization and navigation delivery performance

To achieve the required landing ellipse for Entry Guidance, it was very important that Ground Navigation delivered the spacecraft as close to the nominal trajectory as possible. The larger the error in doing so, the more Entry Guidance would have to work to bring the spacecraft back to the intended landing target. At one point, if the navigation delivery errors are too large, Guidance would start to saturate its control authority and fail to correct for the totality of the error and the spacecraft might land outside the landing ellipse. As it turned out, however, ground navigation performed flawlessly, delivering the spacecraft trajectory to the nominal  $-15.5^\circ$  of Entry Flight Path Angle (EFPA) with an error of only  $0.013^\circ$  against a  $0.2^\circ$  requirement.

In addition to delivering the spacecraft to a given entry state, Ground Navigation had to provide a prediction of the position and velocity of the spacecraft at a predetermined  $T_0$  epoch defined to be 9 min before Entry Interface. This state vector was used to initialize the on-board inertial propagator at the same epoch. After that time, the inertial propagator using attitude-rate and acceleration measurements from the IMU, propagated the position and velocity state which

was used by Entry Guidance to fly the spacecraft to the desired landing target. Errors in the position and velocity knowledge state at  $T_0$  would be invisible to Entry Guidance and would result directly in a landing position error relative to the target. But once again, the performance of Ground navigation was outstanding, with an error in position in the B-plane of 200 m versus a 2.8 km requirement, and an error in velocity of 0.11 versus a 2.0 m/s requirement. What is more, the navigation state that ended up being used by the on-board inertial propagator was uploaded to the spacecraft 6 days before entry. More state knowledge updates were planned as ground navigation produced better estimates, as is expected as the spacecraft gets closer to Mars, with the last opportunity just a few hours before Entry, but the excellent performance of Ground Navigation produced very stable estimates during that period, and updates to the on-board navigation state knowledge were deemed unnecessary.

### 3.2 Attitude knowledge initialization performance

The on-board inertial propagator, in addition to the estimate of position and velocity at  $T_0$ , also needs an estimate of the attitude of the spacecraft at the same epoch. This attitude estimate is provided by the Cruise Attitude Estimator, using

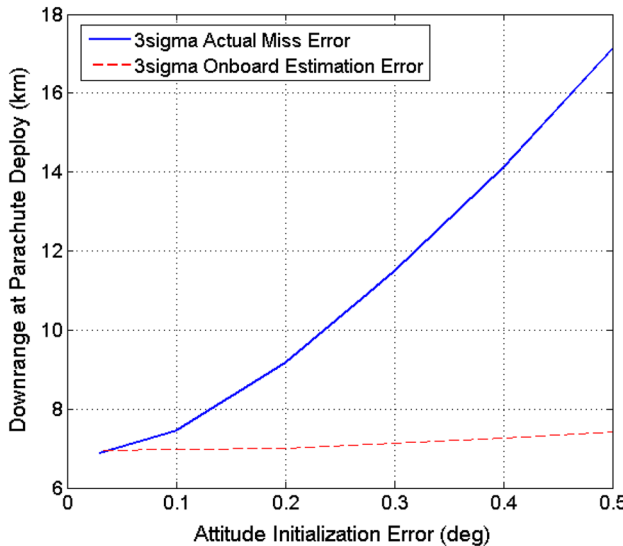


**Fig. 18** Parachute deploy downrange miss distance sensitivity to attitude initialization error

Sun Sensor and Star Scanner measurements. Errors in this attitude estimate results in errors in the inertially propagated position and velocity state that degrades the performance of the velocity triggers and of Entry Guidance, the last resulting in larger landing position errors.

But, the way that attitude initialization errors negatively affect Entry Guidance is a little more subtle than just through errors in the inertially propagated position. The largest guidance performance deterioration occurs through its range predictor, where errors in the estimate of vertical velocity due to errors in the initial attitude estimate result in errors in the predicted range-to-go (1). Errors in the predicted range-to-go lead to errors in the commanded vertical  $L/D$  thorough (2). The large effect of attitude initialization errors can be seen in Fig. 18, where the  $x$ -axis is the size of the attitude initialization error, and the  $y$ -axis show the landing downrange miss distance and the onboard downrange position estimation error. Notice that for large attitude initialization errors, the resulting miss distance is not driven by the direct effect it has in the downrange position estimate but by the error in the estimate of vertical velocity as mentioned before [3].

The large sensitivity of the Entry Guidance performance to the attitude initialization error was a major concern of the EDL team from the beginning of the project and the source of numerous analysis and simulations. This concern was driven by the challenges of calibrating the alignments between the IMU mounted inside the aeroshell and the Sun and Celestial sensors mounted far in the Cruise Stage, which contributed the largest components of the attitude initialization error. For this reason, a very large error,  $0.25^\circ$  3-sigma, was allocated to attitude initialization and all aspects of EDL had to be robust to it. The corresponding

size of the landing ellipse was advertised as 25 by 20 km (major axes), and these numbers were used for landing ellipse placement prior to launch.

During Cruise, the success of the sensor alignment calibration campaign and the good performance of the attitude determination system prompted the EDL team to reduce the estimate of the attitude initialization error from  $0.25^\circ$  to  $0.1^\circ$  3-sigma, and, correspondingly, the size of the landing ellipse to 21 km by 7 km. The smaller landing ellipse size was then used by the project to move its center several kilometers towards Mount Sharp, Curiosity's main science target, to shorten the distance it would have to rove after landing.

Reconstructed performance of the Navigation Filter performance during landing indicated an Attitude Knowledge Initialization error of  $<0.03^\circ$ , almost an order of magnitude smaller than the original requirement.

### 3.3 Entry Guidance performance

First the bottom line: Curiosity landed only 2.2 km east and 400 m north of the target, both less than 1-sigma errors, thus successfully demonstrating the first use of Entry Guidance on Mars.

Because the final landing errors are so small compared to prediction uncertainties, it is hard to tease out from the data the main physics that contributed to it, but this is what we know.

Figure 19 shows the reconstructed Entry trajectory with shaded regions representing the Range Control and Heading Alignment phases [3]. The duration of the entire guided entry was  $<3.5$  min, divided almost equally in half between the two guided phases.

The bottom right plot in Fig. 19 shows the capsule bank angle as a function of time since Entry Interface. In the plot, it can be seen that during Range Control, there were 3 bank-reversals, the nominal number seen in Monte Carlo simulations. During Heading Alignment, the small bank angle zig-zag is due to the Entry Controller deadbands. The  $180^\circ$  bank angle change at 240 s, the end of Heading Alignment is done in preparation for parachute deploy to point the radar beams in a more favorable angle towards the ground.

Combined, the plots in Figs. 20 and 21 provide a good insight into the workings of Range Control. In both figures, the  $x$ -axis in the bottom plot is time since  $T_0$ , 9 min before Entry Interface, and the  $x$ -axis in the top plot is the planet-relative velocity magnitude and flows from left to right in the same direction as time.

In Fig. 20, the  $y$ -axis in both plots depicts the predicted range error defined from (1) and (2) as

$$R_{\text{error}} = R - R_p = (R - R_{\text{ref}}) - \frac{\partial R}{\partial D}(D - D_{\text{ref}}) - \frac{\partial R}{\partial \dot{r}}(\dot{r} - \dot{r}_{\text{ref}}) \quad (5)$$

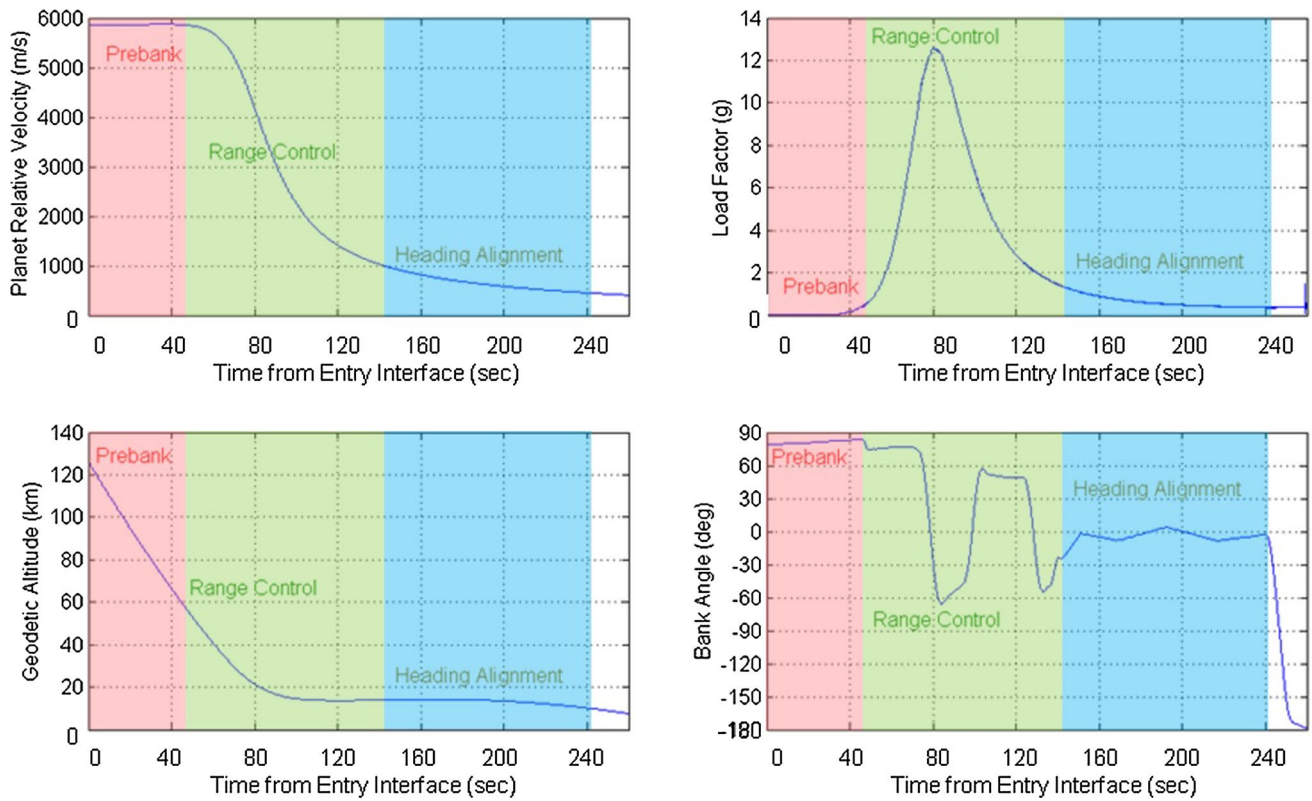


**Fig. 19** Best estimate of the entry trajectory

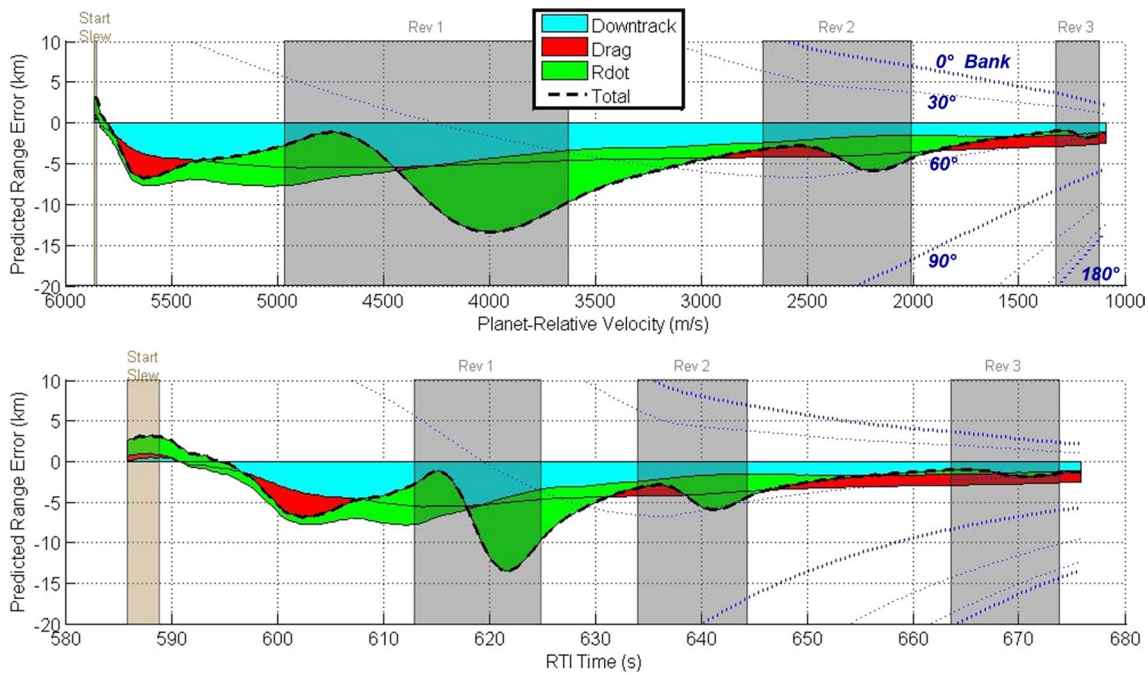


**Fig. 20** Range error components during Range Control

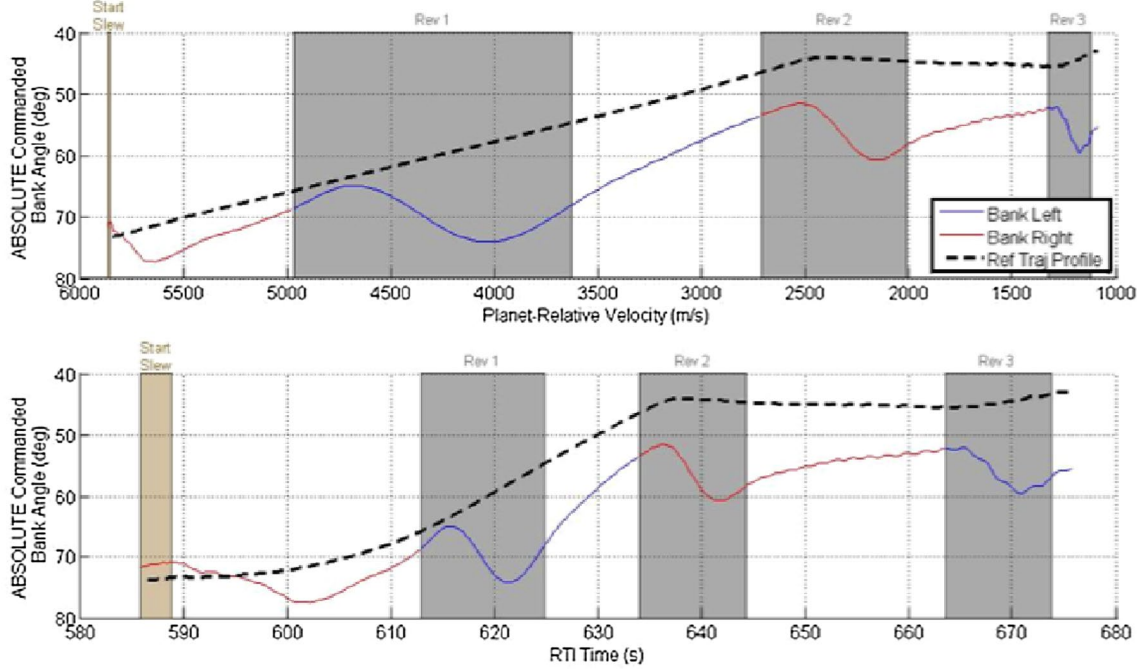


**Fig. 21** Commanded bank angle during range control

and the three additive components that are part of it. The left term is the downtrack error component, shown in the figure in turquoise, and represents the difference between the current range-to-target and the expected one as given by the Reference Trajectory Table at the current velocity. The middle term is the drag error component, shown in the figure in red, and represents the expected deviation in the range-to-target with respect to the reference trajectory due to the difference between the current filtered drag and the expected one from the reference trajectory table at the current velocity. Finally, the right term is the vertical velocity error component, shown in the figure in green, and represents the expected deviation in the range-to-target with respect to the reference trajectory due to the difference between the current vertical velocity and the expected one from the Reference Trajectory Table at the current velocity. The dash line in the figure represents the total predicted error, with positive values indicating landing short of the target and negative landing long. The area plot shows the summation of these components, including how one may cancel another out, in the order shown in the legend.

Figure 21 shows the Commanded Bank Angle from Range Control, with the color depicting whether guidance is commanding negative bank to the left of the plane of motion or a positive bank to the right. The dashed line is the vertical  $L/D$  from the reference trajectory, converted to bank angle using the onboard, filtered  $L/D$  at that time. When the commanded bank magnitude is near the

reference line, there is little predicted range error the guidance is attempting to correct.

Let us go now through an example using the plots of Figs. 19 and 20 to illustrate the behavior of Range Control during the landing of Curiosity. In Fig. 20, we can see that at 5500 m/s there was already a  $-5$  km downtrack error (flying long) that was compounded by an additional  $-3$  km from drag error (less drag than anticipated). The combined  $-8$  km deficit was partially compensated by a  $+2$  km predicted range error due to vertical velocity error (more down-vertical velocity than anticipated) for a total predicted range error of  $-6$  km. In Fig. 21, we can see that Entry Guidance compensated this predicted range error by commanding a larger bank angle than the reference, resulting in less vertical lift, which resulted in an increased down-vertical velocity. As the trajectory encountered a thicker atmosphere at lower altitudes, the component of predicted range error due to drag started to decrease. By the time the spacecraft reached 4750 m/s, the drag error component was reduced to  $-1$  km, the downtrack error component had stopped growing at  $-6$  km, and the vertical velocity component of  $+6$  km almost brought the total predicted range error to zero. Right after that, however, the ongoing bank-reversal applied too much vertical lift and the vertical velocity component grew in the opposite direction and changed sign, and by 4000 m/s it contributed more than  $-7$  km, for a total of  $-13$  km predicted range error. Entry guidance responded quickly thanks to the over control gain  $K_3$

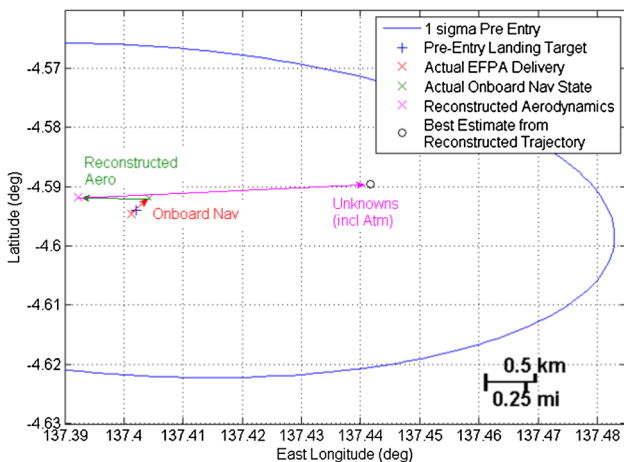


**Fig. 22** Landing error at touchdown contributors

in (2) by reducing lift by increasing the commanded bank angle away from the reference, as can be seen in Fig. 21, and achieving the largest bank angle at 4000 m/s. By the time of the start of the next bank-reversal, Range Control had removed most of the predicted range error due to the vertical velocity component introduced in the previous one. During the second bank-reversal, the same expected behavior occurs as the first but with lower magnitudes due to lower decelerations.

Along the Range Control Phase, we can see an almost steady reduction in the long downrange error component (turquoise in Fig. 20) thanks to the guided corrections of both drag and vertical velocity integrated over time. By the end of the range control phase, the downtrack error component is near  $-3$  km, the drag error component is near  $+1$  km and the  $r$ -dot error component is nearly 0. This results in a final predicted range error near  $-2$  km, which represents about a 1-sigma value from the pre-landing prediction statistics. It is clear that the final bank-reversal introduced some additional predicted range error further downrange, as expected, and that there was not enough time left during the range control phase to significantly reduce that impact. This late reversal behavior was common to the pre-flight Monte Carlos and was already accounted in the tuning of the parachute deploy range bias parameter.

To determine what were the dominant errors that contributed to the 2.2 km miss distance, a series Monte Carlo simulations were made, where dispersed variables were replaced by reconstructed undispersed ones where possible: Initial Attitude Knowledge error, Navigation Delivery error, On-board Navigation State Knowledge error, and aerodynamics [3]. The result of this work is shown in Fig. 22. We can see that both navigation errors, delivery and on-board navigation state, contributed very little

in explaining the landing error. The reconstructed aerodynamics actually contributed to the deficit by moving the center of the ellipse to the west about 0.6 km. This leaves an unexplained 2.9 km error due east. At this point, the most likely explanation is tail winds starting at close to the end of guidance [3]. This theory is supported by the uncharacteristically long time it took between the activation of two velocity triggers: the one that starts the preparations for chute deployment at the end of Heading Alignment and the one that triggers the chute deployment a few seconds later.

### 3.4 Entry controller performance

In telling the story of the Entry Controller reconstructed performance, it is almost as important to tell what did not happen as much as what did. Through the development of MSL EDL, we encountered a couple of technical challenges that could threaten the performance of the Entry Controller. The first was the potential adverse interaction between the supersonic flow and RCS firings, called Aero/RCS interactions for short, which in its worst manifestation can result in a reversal of the control action with possible catastrophic results. These fears were fueled by the experience of the first Space Shuttle flight where this effect was encountered, requiring the crew to take control from the autopilot. The Phoenix Mars lander also encountered this problem during development and chose to fly with their controller deadbands wide open to minimize the chance of firing RCS thrusters. The MSL EDL team researched and studied the aero/RCS interaction problem in detail, leading ultimately to the change in the location and pointing directions of the RCS thrusters in the aeroshell, to increase their moment arms and reduce the interactions with the aerodynamic flow [9].

The second technical challenge was associated with the potential existence of aerodynamic roll torques that might reduce, or even overwhelm, the control authority needed to maintain the desired bank angle. Since the capsule is symmetric about the roll axis, one has to propose a mechanism to break that symmetry to create such torque. The most credible one was the asymmetric loss of tiles in the heatshield. Again, the EDL team performed extensive analysis and simulations to bound and model this effect in the simulations. Thankfully, the increased control authority resulting from changing the configuration of the thrusters to mitigate the Aero-RCS interaction problem also helped with this one. In addition, a new Entry Controller mode was implemented that gave up coordinated turns (turns about the trim axis of the capsule) for increased roll control authority, at the expense of sideslip errors, which was only activated if the roll control errors exceeded a very large value.

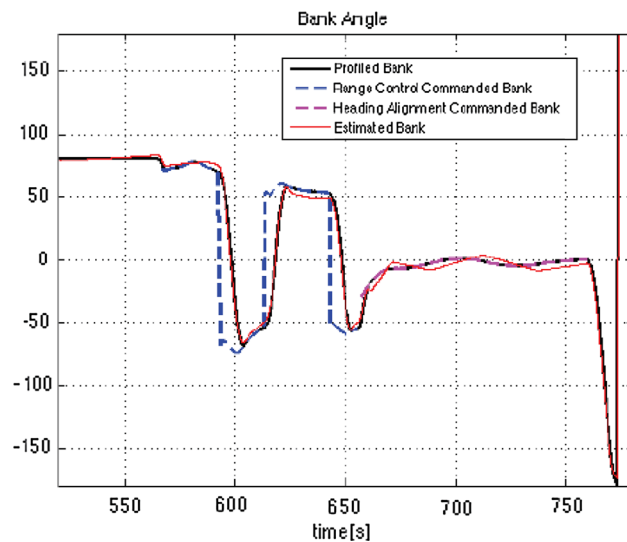


**Fig. 23** Bank angle in degrees during entry

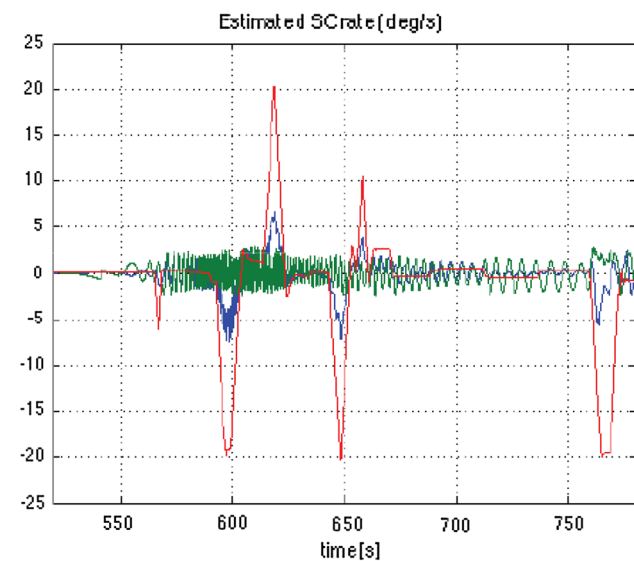
Both these aerodynamic effects were incorporated in the aerodynamic database used by the post Monte Carlo simulation. Despite the conservativeness of the models, the performance of EDL met all the requirements with ample margin.

Figure 23 shows a plot of the bank angle as a function of time, starting at Entry Interface and ending at parachute deploy. There are three lines in this plot. The dashed line is the bank angle commanded by Entry Guidance, blue during Range Control and purple during Heading Alignment. The solid black line is the profiled bank angle generated by the Attitude Profiler and that is the input to the Attitude Controller. Finally, the solid red line is the estimated bank angle. The difference between the solid red line and the back one is the bank angle control error.

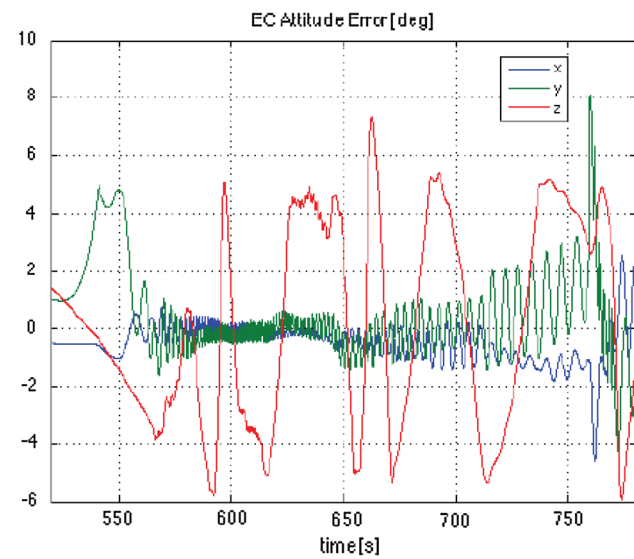
In Fig. 23, we can see the discontinuities in the commanded bank angle (dashed blue) at the bank-reversals. At 780 s, we can see the 180° slew to improve the radar view geometry prior to parachute deployment also known as the Straighten-Up-and-Flight-Right (SUFR) maneuver.

Figure 24 shows a plot of the angular rates during the same period of flight. The red line corresponds to the roll axis while the blue line corresponds to the side-slip (beta) axis and the green to the angle-of-attack (alpha) axis. In the red line, one can easily see the maximum bank angle rate of 20°/s during the bank-reversals and the SUFR maneuver.

Figure 25 shows the attitude control errors. We can see that the bank control error (red line) is mostly contained within the 5° deadbands, and the behavior within the deadbands does not indicate the evidence of any significant disturbance torques. The side-slip control error (blue line) develops a  $-1.7^\circ$  bias above 720 s, which is thought to be due to a cross-wind, but it stays far from the



**Fig. 24** Capsule angular rates in degrees/second



**Fig. 25** Attitude control errors in degrees

10° deadband. Likewise, the angle-of-attack control error (green line) develops a bias of up to  $+1.8^\circ$ , but also stayed far away from the 10° deadband. This last error remains unexplained.

Fuel usage was nominal at about 12 kg. No discernable Aero-RCS interaction and roll-torque effects were present. The Entry Controller performance was excellent.

### 3.5 Powered Descent performance

Powered Descent is perhaps of all the EDL phases the riskiest, and in MSL, with the inclusion of the SkyCrane,

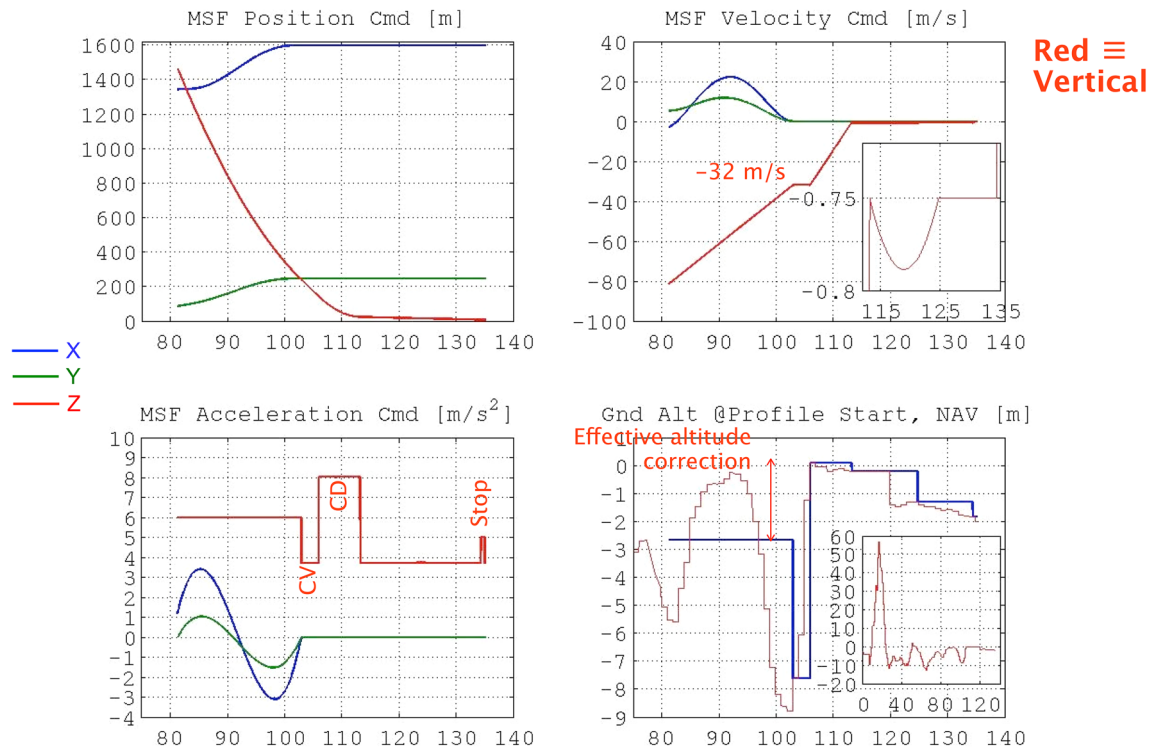


**Fig. 26** Powered Descent position, velocity, acceleration, and ground altitude vs. time

is even more risky. It is worth reminding the reader at this point that no hot-fire test of the SkyCrane had been conducted prior to landing on Mars; we had only conducted analysis, unit level testing (e.g. radar, bench thruster testing, structural model surveys, bridle characterization, etc.), and end-to-end high fidelity simulations [10, 11].

The good news is that Powered Descent, including the SkyCrane, performed extremely well, with only few issues that are too small to be worth explaining in this paper, and a significant one mentioned here first but explained in detail in the next section on Navigation Filter performance.

Backshell separation occurred at 1.67 km altitude while traveling at a vertical velocity of 78.7 m/s and a horizontal velocity of 6 m/s. This compares extremely well with respect to the expected values of 1.6 km altitude, 80 m/s vertical velocity, and 6.3 m/s horizontal velocity. The full duration powered flight was 55.2 s.

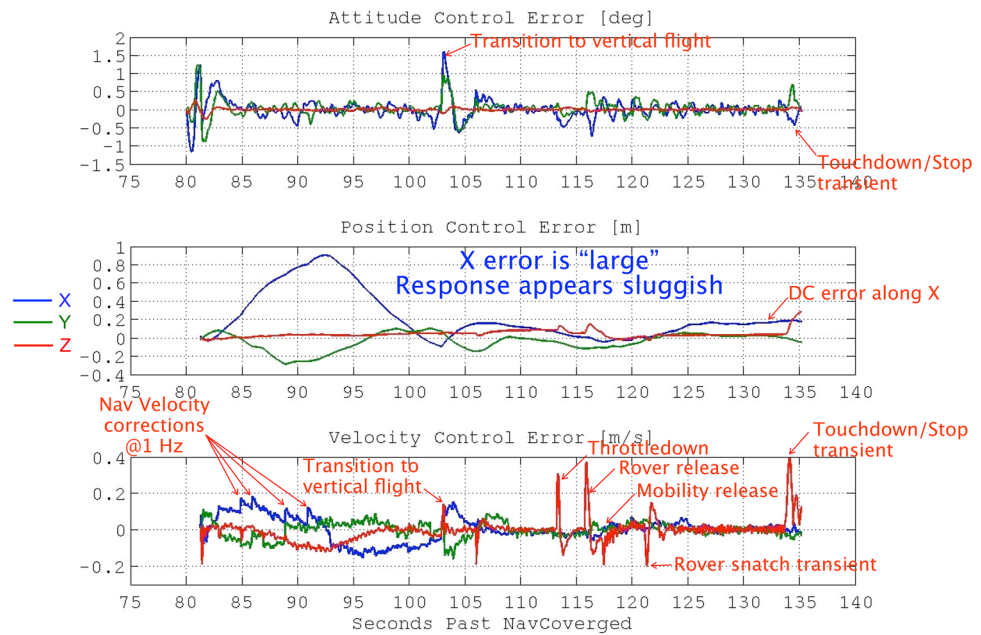
The altitude loss during Constant Velocity phase, the accordion phase used to heal altitude knowledge, was 97 m against a nominal 100 m. This means that the on-board altitude estimate at Powered Descent start was in error by only 3 m, which is almost an order of magnitude less than the expected 3-sigma value given the topography of the landing site.

Figure 26 shows several important plots associated with Powered Descent. For all the plots, the  $x$ -axis is time in seconds since Navigation Filter convergence. The top left

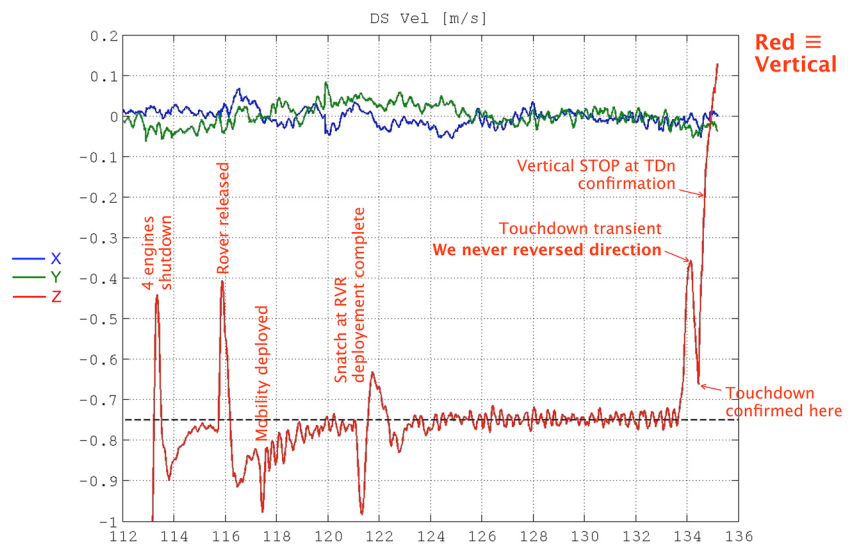
plot is the position of the spacecraft in the Mars Surface Fixed (MSF) frame where  $x$ -axis is pointing east, the  $y$ -axis is pointing north, and the  $z$ -axis is pointing up. The origin of this frame is on the surface of the planet vertically below the spacecraft at the time of Nav Filter convergence. In this plot, the 300 m divert maneuver used to avoid spacecraft re-contact with the parachute and backshell can be seen between 81 and 103 s.

The top right plot in Fig. 26, shows the velocity of the spacecraft relative to the ground, also in the MSF frame. The constant 32 m/s Constant Velocity mentioned above is clearly seen. The bottom right plot deserves an explanation first. The Navigation Filter propagates the position of the spacecraft using the IMU and the TDS Doppler velocity measurements only. A separate filter computes the altitude of the ground in the MSF frame, as derived from the TDS altimeter measurements and the estimate of the spacecraft position mentioned above. The estimate of the spacecraft altitude relative to the ground is then computed by differencing the  $z$ -axis component of the estimate of position of the spacecraft and the estimate of the altitude of the ground. The bottom right plot in Fig. 26 shows the Navigation Filter estimate of the altitude of the ground as a function of time. The solid blue lines represent the values of that ground altitude used by Powered Descent guidance at the beginning of each phase to generate the corresponding reference trajectory profile. The bottom line here is that

**Fig. 27** Powered Descent control errors



**Fig. 28** Descent Stage velocity during SkyCrane



the changes in the estimate of the ground altitude (due to TDS altimetry errors and terrain relief, etc.) are negligible with respect to the 100 m Constant Velocity accordion designed to handle the changes.

Figure 27 shows the attitude, position, and velocity control errors for the entire duration of powered flight. No instabilities or pendulum dynamics can be noticed. The magnitudes of the control error transients during major dynamic events (i.e., throttle-down, rover separation, touchdown, etc.) are within expectation, and the control system transient recovery time was also as expected. The low frequency  $x$ -axis position control errors, however, are a little bit of a mystery. After some analysis, the 1 m excursion during Powered Approach might be the result of

Navigation Filter velocity estimate corrections as it processes radar data, all correcting in the same direction during the error growth. That would not explain, however, the 0.15 m  $x$ -axis position control error bias developed during the SkyCrane. A possible explanation of the last one, is a  $0.18^\circ$  change in the combined direction of the thrust provided by the engines, which corresponds to only 20 N of force.

Figure 28 shows in more detail the estimated velocity of the Descent Stage during the critical SkyCrane maneuver. Notice that at the instant of touchdown, the estimated velocities are way below the 0.1 m/s requirement from the nominal of 0.75 m/s vertical velocity and zero horizontal velocity, not surprisingly given the small velocity control

errors in Fig. 27. Again, the transients are as expected and no evidence of pendulum dynamics (7 s period) can be seen.

Fuel usage was lower than expected and given the data available, it is difficult to pin-point the cause with certainty. It is believed that a combination of better MLE ISP and an MLE throttle calibration error of a few percentage points is the most likely explanation [7].

### 3.6 Navigation Filter performance

Navigation Filter Convergence occurs when the filter has processed enough good radar measurements (i.e., consistent with the IMU propagated state) to generate the first navigation solution, indicating for the first time, and by direct measurement, the altitude and 3-axis velocity of the spacecraft relative to the ground. Without Navigation Filter convergence, the mission is an assured failure. Hence, this is an event always awaited with a great deal of anxiety by all EDL teams as they follow the real-time telemetry. During MSL landing, the news could not have been better. Navigation Filter convergence occurred at 8.3 km altitude, a 3.8-sigma higher than the 6.8 km mean of the pre-landing generated statistics. What was even more surprising, however, was that the first Navigation Filter solution indicated that the error in the IMU-propagated-state, estimated from landing radar measurements, was only 0.77 m/s in velocity and 113.4 m in altitude. These errors were the result of several error contributions such as ground navigation error in the initial translation state, attitude initialization error, IMU measurement error, TDS measurement error, and on-board gravity model error. If the IMU-propagated-state errors were blamed on attitude initialization error only, the attitude initialization error would have to be smaller than  $0.010^\circ$ , or 25 times lower than the  $0.25^\circ$  requirement mentioned before!

The Navigation Filter estimation of the coordinates where the rover landed was 770 m off as compared to the true location obtained from Mars Reconnaissance Orbiter (MRO) pictures. After correcting the on-board estimate with the latest orbit determination solution before landing (recall that the on-board navigation state was uploaded to the spacecraft 6 days prior to landing and not updated after that because the errors were too small to be worth the effort and risk) this number came down to 162 m, thus confirming once again the excellent attitude initialization and IMU performance.

On the downside of things, perhaps the biggest surprise of the EDL reconstruction was what was learnt from Fig. 29. The MSL Navigation Filter, unlike a regular Kalman Filter, after estimating the error in IMU-propagated velocity from radar measurements, it does not correct the IMU-propagated state with it but keeps it separate. When, for example, the Powered Descent Controller requires the

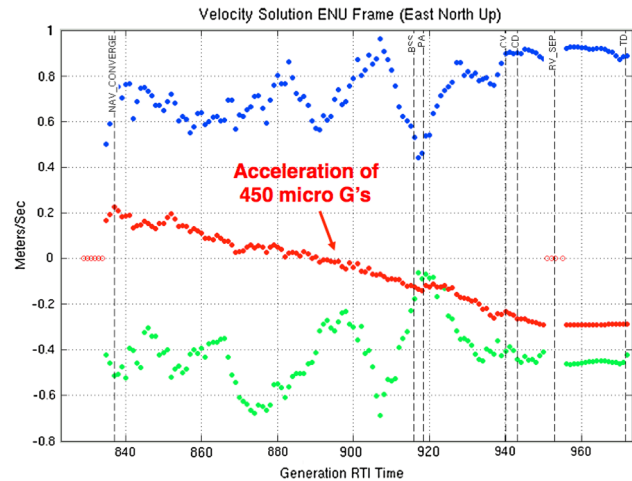


**Fig. 29** Navigation Filter velocity corrections estimates

latest spacecraft velocity estimate from the Navigation Filter, the filter takes the current IMU-propagated state and corrects it with the latest estimate of the velocity errors. Figure 29 plots the velocity estimation errors in a North, East, Up frame as taken from telemetry. If the IMU was perfect and have been initialized with perfect attitude, and the gravity model was also perfect, we would expect those errors to be not necessarily zero but perfectly flat. However, if we introduced an attitude initialization error, we would expect that the horizontal channels (blue and green) would have a ramp with a slope equal to the attitude error times Mars gravity ( $\sim 3.7$  m/s). As can be seen, the horizontal channels have very little slope, confirming once again the small attitude initialization error. The vertical channel (red line), on the other hand, has a significant slope:  $\sim 4.5 \times 10^{-3}$  m/s<sup>2</sup>. This acceleration is too large to be accelerometer bias (acceleration bias calibration during Cruise estimated the bias to be a factor of four or more smaller). The only other possibility was an error in the on-board gravity model.

The on-board gravity model is a simple J2 model. Extensive Monte Carlo simulations using high fidelity gravity models indicated that the on-board J2 model was good enough in the landing sites that were considered early in the mission. The only remaining possibility was a gravity anomaly at the floor of Gusev crater, which was exactly what turned out to be. In Fig. 30, we can see gravity anomaly errors of up to  $3.7$  mm/s<sup>2</sup> in Curiosity's landing site.

Given this new information, it was clear that the velocity estimates reported by the Navigation Filter during landing had some significant errors. In particular, the concern was during the SkyCrane phase when only the two  $50^\circ$  radar beams were used by the Navigation Filter (because of the concern of RF interference on the other beams by the rover which was near or in their path), which forced the propagation of the vertical channel on the IMU only.

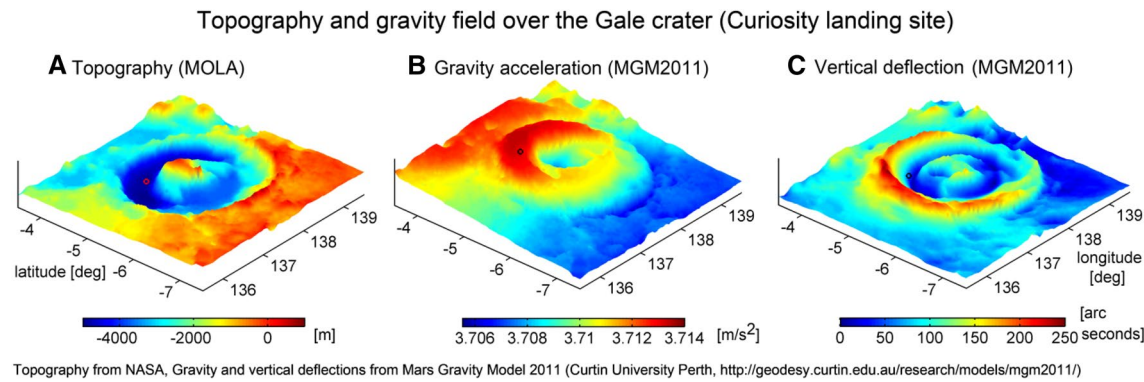


**Fig. 30** Gale crater gravity anomaly

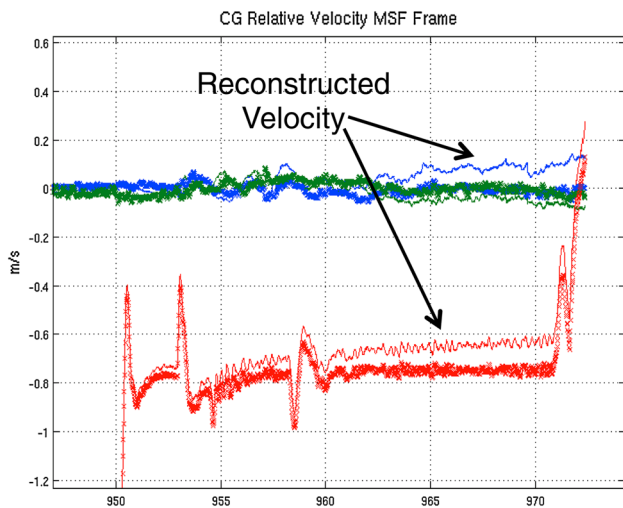


**Fig. 31** Original and reconstructed velocity

To reconstruct the actual state of the spacecraft during landing, the Navigation Filter was run stand-alone with the IMU and radar measurements that were collected as telemetry during landing and with a compensating bias in the gravity model to remove the slope in the vertical channel as shown in Fig. 29. The results can be seen in Fig. 31, where two sets of velocities are plotted: the original from flight telemetry and the post-landing reconstructed. As can be seen in the plot, Curiosity landed more than 0.1 m/s slower than the nominal 0.75 m/s. While a lower touchdown velocity is better for the rover, the number represents more than a 3-sigma error when compared to predictions.

The slower vertical velocity was consistent with the unusually long time that elapsed between the time touchdown was expected and when it happen, thus giving credence to the validity of the reconstruction.

The error in the on-board gravity model also resulted in errors in horizontal velocity, as the vertical velocity error coupled through the estimator into the other channels

(Fig. 31), resulting in a touchdown horizontal velocity of more than 0.1 m/s, also a larger than 3-sigma event but of little consequence to the success of the mission.

While the gravity anomaly contributed the bulk of the Navigation Filter velocity estimation error, there was a second undesirable, yet not unexpected, error source: noisy TDS velocity measurements due to dust blown from the Mars surface by the MLE engine plumes as it got close to touchdown. This effect was clearly seen during the helicopter field tests of the TDS while flying over sand dunes in the Mohave Desert, spawning a flurry of activities to understand and predict the degree to which it could occur on Mars.

The basic physics of the problem were relatively straightforward: the radar measures an energy-weighted average between its true ground velocity and that of the sand particles. The hard part was to predict to what degree the MLE engines might pick up dust on Mars and at what speeds. It was felt, qualitatively, that the helicopter tests on sand dunes represented an upper bound on this undesirable effect, one reason for that being that the radar TDS beams used by the Navigation Filter in the last 23 m of altitude, the SkyCrane antennas, were canted 50° away from the MLE's plumes, which was an attenuating factor when compared to the helicopter configuration.

To quantify and bound this issue, analyses were performed based on work on the interaction of rocket plumes with lunar surfaces, done during the sixties, to support the Apollo project. The result of the study was a bound that predicted that this problem was going to be minimal on landing day at Mars. As it turned out, however, the resulting effect was large enough to be observed and affect slightly (~0.05 m/s) the estimated horizontal velocity [12]. Figure 32 shows the measurement residuals belonging to the last 350 measurements from the SkyCrane antennas once the effect of the gravity anomaly and the “bad” measurements themselves were removed. The zero index in the x-axis represents the last measurement and, therefore, the lowest altitude. As you can see, the number of anomalous

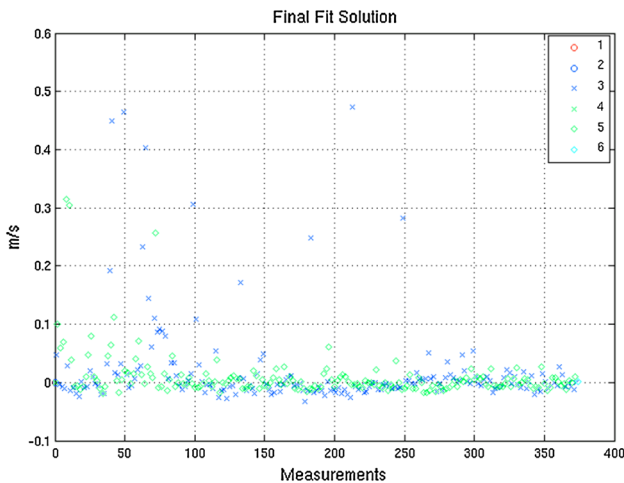


**Fig. 32** Velocity residuals of TDS measurements (SkyCrane antennas)

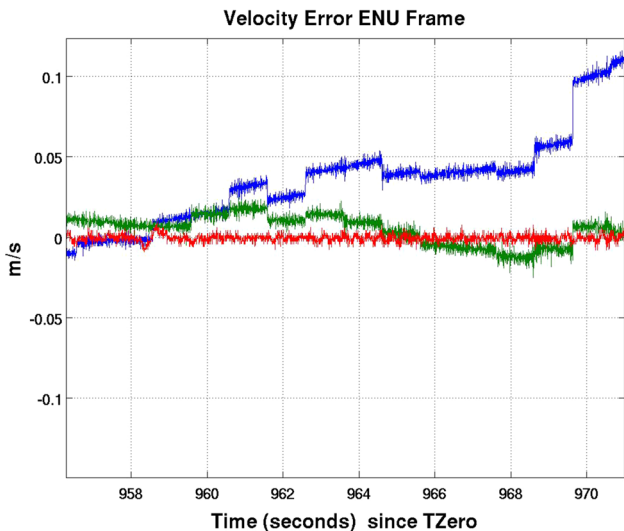


**Fig. 33** Reconstructed Navigation Filter velocity estimation error with gravity anomaly compensated

measurements, believed to be due to dust effects, is small and increases in frequency at lower altitudes.

To quantify the effect of these “bad” measurements on the estimated velocity, a reconstruction of the state of the Descent Stage was generated starting with the final state of the rover on the surface of Mars (i.e., zero ground velocity) and propagating backwards through the touchdown event using the rover LN200 IMU until before Rover Separation when the LN200 and the MIMU were rigidly connected to each other. At this point, the state knowledge of the Descent Stage was propagated forward using MIMU measurements and the initial state from the LN200 backwards propagation.

Figure 33 shows the error in the Descent Stage velocity estimate generated by running the Navigation Filter

stand-alone with flight MIMU and TDS measurements and with the gravity anomaly compensated, as computed from the reconstructed “true” state generated by the procedure described above. The jumps in the figure are the result of the Navigation Filter ingesting the bad measurements, which contributed about 0.05 m/s horizontal velocity error at touchdown.

## 4 Future Mars EDL/GN&C improvements

While the flight performance of MSL EDL/GN&C was excellent and had very few performance surprises, there is always room for improvements. In this section, we will describe three classes of possible improvements to Mars EDL/GN&C.

### 4.1 Fixes to the MSL design

The proposed Mars 2020 mission would improve the performance of the Navigation Filter during touchdown by (a) adding gravity bias correction parameters to enable tuning the Navigation Filter gravity model to the local gravity of the selected landing site, and (b) tuning the Navigation Filter to edit-out TDS measurements corrupted by the moving sand during the SkyCrane phase.

The proposed gravity bias correction parameter solution to the gravity anomaly issue encountered by MSL allows us to match the low altitude local gravity of the selected landing site during the time it is most critical (i.e., SkyCrane phase) without having to increase the on-board gravity model to the inordinate degree that would be required to capture such local gravity effects.

As far as the anomalous TDS velocity measurements during SkyCrane, the MSL Navigation Filter design included a very effective data-editing algorithm but it was tuned to edit-out only very pathological measurements that could significantly affect the touchdown velocity. Mars 2020, however, is planning to tighten the thresholds of the data editor to reject anomalous measurements like the ones encountered by MSL. To evaluate this option, the Navigation Filter was re-run in stand-alone mode with TDS and MIMU measurements from the MSL landing, the gravity anomaly compensated, and the tighter data-editing thresholds. Figure 34 shows the resulting estimated velocity errors, which exhibit a significant improvement when compared to the results of Fig. 33.

### 4.2 Potential functional improvements for Mars 2020

The proposed Mars 2020 mission is considering two potential GN&C enhancements to improve landing accessibility to scientifically interesting sites. The enhancements are:

*Reduce the size of Landing Ellipse* The MSL’s parachute deploy trigger design was based on the principle of opening

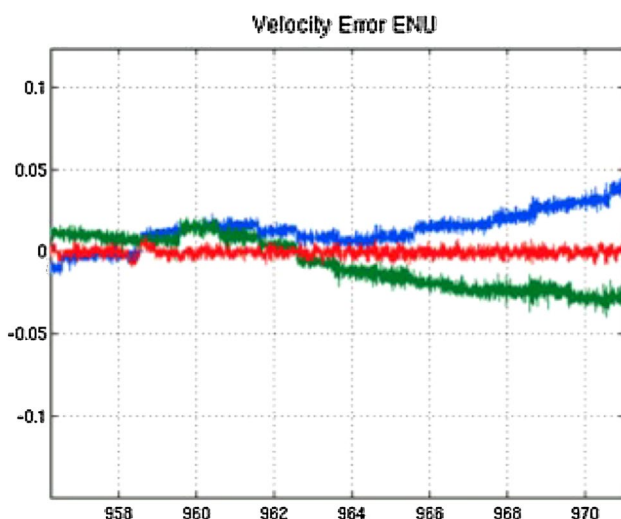


**Fig. 34** Reconstructed Navigation Filter velocity estimation error with gravity anomaly compensated and tighter data-editing thresholds

the parachute as soon as it is safe to do so as not to lose altitude and thus maximizing the accessibility of the system to higher altitude landing sites. For the type of trajectory followed by a lifted entry capsule, like the MSL design, the Mach number is the right indicator to signal that it is safe to open the parachute. Since we do not have a Mach sensor on-board, we use MIMU propagated velocity instead and a velocity threshold value that takes into account the error in the conversion to Mach number (atmospheric temperature, winds, navigated velocity error, etc.).

An important characteristic of this parachute deploy trigger design is that it does not take into account the position of the capsule with respect to the landing site in its logic. This “deficiency” is compensated by Entry Guidance whose only purpose is to make sure that the parachute deploy conditions (i.e. Mach number) are achieved when the spacecraft is at the right place relative to the targeted landing coordinates.

This approach allowed MSL to make a quantum leap in the reduction of the landing ellipse relative to previous Mars landers.

To make a further improvement on the size of the landing ellipse, Mars 2020 is considering replacing the parachute deploy velocity trigger with a downrange error trigger to eliminate any remaining guidance error along track. It is estimated that this approach can reduce the major axis of the landing ellipse from 20 to 12 km, resulting in a 40 % decrease in landing ellipse area size at the cost of about 0.5 km of landing site altitude capability.

*Reduce the engineering hazard requirements on Landing Ellipse* MSL required that, probabilistically, the number of landing hazards inside the selected landing ellipse was negligibly small. Mars 2020 is considering relaxing this

requirement by adding Terrain Relative Navigation (TRN) and Multi-Point Divert capability. In this approach, TRN is used while the spacecraft is still on the parachute phase, to determine with great accuracy the position of the spacecraft in a Mars referenced coordinate frame, and that knowledge is then used to find the closest safe landing site, or point, from an on-board catalog of landing hazards. During powered descent, the spacecraft diverts its trajectory to land in that safe point. This multi-point divert has the capability to divert to larger distances and hence avoid landing hazards of up to 110 m in radius. This capability takes advantage of unallocated fuel and stays within the MSL fuel control authority constraints.

The TRN capability will be provided by the Lander Vision System (LVS), which is explained in great detail in [13].

#### 4.3 Functional improvements and enhancements beyond Mars 2020

##### 4.3.1 Hazard detection and avoidance

To have accessibility to even more challenging landing sites over what is planned for Mars 2020 will require the use of autonomous Hazard Detection and Avoidance (HD&A). The preferred sensor to achieve this functionality is 3D-LIDAR. In particular, Flash LIDAR is being considered as the best sensor option given the high dynamics and short time present in Mars EDL [13]. NASA’s ALHAT program is studying the same technology for lunar landing applications [14].

##### 4.3.2 Powered Descent large divert guidance

Future missions to Mars will eventually have to solve the pin-point landing problem where the required size of

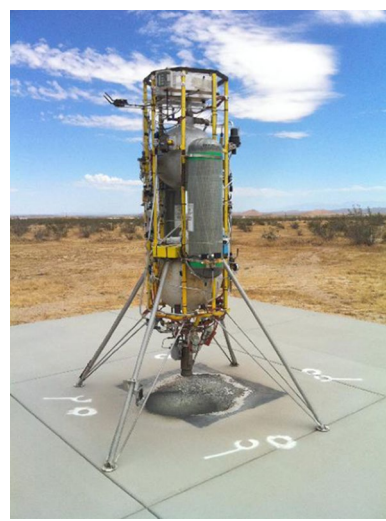


**Fig. 35** Descent and Ascent Powered-flight Testbed (ADAPT)

the landing ellipse is in the tens of meters. This would require about the same level of TRN capability that Mars 2020 is planning to demonstrate with LVS, but the size of the divert maneuver required during Powered Descent to fix the remaining guidance errors at the start of this phase will be dramatically larger, reaching up to several kilometers. The Apollo derived polynomial guidance of MSL is not fuel efficient enough to do the job and new guidance laws are being developed. To achieve the fuel optimality while respecting all the practical constraints present in a Mars Powered Descent Phase (sensors FOV, maximum velocities, terrain variations, min and max control authority, etc.), guidance laws using convex optimization has been developed at JPL. The Guidance for Fuel Optimal Large Diverts (G-FOLD) is real-time implementable with current flight processors [15, 16] and is being demonstrated in the Autonomous Descent and Ascent Powered-flight Testbed (ADAPT) using a propulsive free-flyer from Masten Space Systems (Fig. 35) [17].

## 5 Conclusions

MSL EDL represented the largest jump in Mars EDL performance since Viking. To reduce the size of the landing ellipse, MSL had to implement for the first time Entry Guidance on another planet. In addition, to accommodate a rover weighing almost 1 ton and with the size of a small car, MSL had to invent and develop a totally new landing architecture: the SkyCrane. This paper first describes the salient elements of the design of the EDL Guidance, Navigation, and Control system, and then how it performed in flight during Curiosity's landing in August 5, 2012.

Overall, the performance of MSL EDL was outstanding, landing at 2.2 km away from the target well within the  $21 \times 7$  km predicted landing ellipse. The SkyCrane performed just as advertised, and the touchdown velocities while falling outside expectations did not endanger either the rover or the mission.

Margins were very healthy in most areas, showing the robust "kill it with margin" MSL design philosophy. The gravity anomaly surprise can be easily fixed in future missions, like Mars 2020, by simply adding a bias correction parameter to the J2 gravity model that is based on the local Mars gravity models of the landing site itself.

The paper concludes with a summary of future short and long term enhancements to the MSL EDL/GN&C design.

**Acknowledgments** The authors would like to thank Adam Steltzner (JPL), David Way (LaRC), Jody Davis (LaRC), Lynn McGrew (JSC), Allen Chen (JPL), Steve Sell (JPL), Devin Kipp (JPL), and Ray Baker (JPL) for providing materials and consultation for this paper, as well

as to the rest of the MSL EDL team that were an integral and essential part of the success of Curiosity's landing.

**The work was performed at the Jet Propulsion Laboratory, California Institute of Technology, under contract with the National Aeronautics and Space Administration. © 2014 California Institute of Technology. Government sponsorship acknowledged.**

## References

1. Steltzner, A.D., San Martin, A.M., Rivellini, T.P., Chen, A.: Mars science laboratory entry, descent, and landing system overview and preliminary flight performance results. AAS 13-236, AIAA/AAS Space Flight Mechanics Meeting, Lihue, HI (2013)
2. San Martin, A.M., Lee, S.W., Wong, E.C.: The Development of the MSL Guidance, Navigation, and Control System for Entry, Descent, and Landing. AAS-13-238, AIAA/AAS Space Flight Mechanics Meeting, Lihue, HI (2013)
3. Mendeck, G.F., McGrew, L.C., AAS-13-419: Post-flight EDL entry guidance performance of the 2011 Mars science laboratory mission. AAS/AIAA Space Flight Mechanics Meeting, Kauai, HI (2013)
4. Chen, A., Beck, R., Brugarolas, P., et al.: Entry system design and performance summary for the Mars science laboratory mission. AAS 13-422, AIAA/AAS Space Flight Mechanics Meeting, Lihue, HI (2013)
5. Baker, R., Casillas, A.: MSL Descent Stage integrated propulsion subsystem: development and flight performance. AAS 13-462, AIAA/AAS Space Flight Mechanics Meeting, Lihue, HI (2013)
6. Brugarolas, P.B., San Martin, A.M., Wong, E.C.: The entry controller for the Mars science laboratory. AAS/AIAA Space Flight Mechanics Meeting, Kauai, HI (2013)
7. Dyakonov, A.A., Schoenenberger, M., Scallion, W.I., Van Norman, J.W., Novak, L.A., Tang, C.Y.: Aerodynamic Interference Due to MSL Reaction Control System. In: 41st AIAA Thermophysics Conference, San Antonio, Texas, June 2009
8. Singh, G., San Martin, A.M., Wong, E.C.: Guidance and control design for powered descent and landing on Mars. IEEE AC paper #1548, Version 2, Updated 11 Dec 2006
9. Sell, S., Chen, A., Davis, J., San Martin, A.M., Serricchio, F., Singh, G.: Powered flight design and reconstructed performance summary for the Mars science laboratory mission. AAS/AIAA Space Flight Mechanics Meeting, Kauai, HI (2013)
10. Way, D., Davis, J., Shidner, J.: Assessment of the Mars science laboratory entry, descent, and landing simulation. AAS 13-420, AIAA/AAS Space Flight Mechanics Meeting, Lihue, HI (2013)
11. Way, D.: Preliminary assessment of the Mars Science Laboratory entry, descent, and landing Simulation. IEEE-2013-2755, IEEE Aerospace Conference, Big Sky, MT, March 2013
12. Chen, C., Pollard, B.: Radar terminal descent sensor performance during Mars science laboratory landing. A32641, J Spacecr Rocket (**in press**)
13. Johnson, A., Bergh, C., Cheng, Y., Clouse, D., Gostelow, K., Ishikawa, K., et al.: Design and Ground Test Results for the Lander Vision System. In: AAS 13-042, 36th Annual AAS Guidance and Control Conference, Breckenridge, Colorado, Feb 2013
14. Trawny, N., Carson, J.M., Huertas, A., Luna, M.E., Roback, V.E., Johnson, A.E., Martin, K.E., Villalpando, C.Y.: Helicopter Flight Testing of a Real-Time Hazard Detection System for Safe Lunar Landing. In: Proceedings AIAA SPACE 2013 Conference and Exposition, San Diego, California, Sept 2013

15. Blackmore, L., Açıkmese, B., Scharf, D.P.: Minimum landing error powered descent guidance for Mars landing using convex optimization. *J. Guid. Dyn. Control.* vol. 33(4), (2010)
16. Acikmese, B.B., Ploen, S.R.: A convex programming approach to constrained powered descent guidance for Mars pinpoint landing. *J. Guid. Dyn. Control.* vol. 30(5), (2007)
17. Scharf, D.P., Regehr, M.W., Dueri, D., Acikmese, B., Vaughan, G.M., Benito, J., Ansari, H., Aung, M., Johnson, A., Masten, D., Nietfeld, S., Casoliva, J., Mohan, S.: ADAPT Demonstrations of Onboard Large-Divert Guidance with a VTVL Rocket. In: *IEEE Aerospace Conf.*, 2014